Evolutionary Intelligence (2024) 17:653–678
https://doi.org/10.1007/s12065-022-00804-0

REVIEW ARTICLE

Solving multi-objective truss structural optimization problems considering natural frequencies of vibration and automatic member grouping

Érica C. R. Carvalho[1] · José Pedro G. Carvalho[2] · Heder S. Bernardino[3] · Afonso C. C. Lemonge[4] · Patrícia H. Hallak[4] · Dênis E. C. Vargas[5]

Received: 2 August 2022 / Revised: 28 October 2022 / Accepted: 20 November 2022 / Published online: 13 December 2022

Abstract
Minimizing the mass of a structure and maximizing its first natural frequency of vibration are conflicting objectives of real interest in structural design. To avoid problems with resonance, which can lead to their collapse, structures can be designed by making the first natural frequency of vibration high. Furthermore, it is crucial to stay away from excitation frequencies. Here we formulate and solve multi-objective structural optimization problems of trusses with these conflicting objectives. This type of problem is uncommon in the literature, since the natural frequencies of vibration are generally set as constraints rather than as objective functions. The generalized differential evolution 3 (GDE3), the nondominated sorting genetic algorithm II (NSGA-II), decision space-based niching (DN-NSGA-II), the competitive mechanism-based multi-objective particle swarm optimizer (CMOPSO), and the MOPSO with multiple search strategies (MMOPSO) are the algorithms used in this paper. Additionally, cardinality constraints are used to manage the difficulty of discovering the best member grouping, which is very effective in addressing the problems analyzed in this paper. The experiments refer to the 10-, 25-, 72-, and 200-bar trusses. Each involves two analyses, taking into account the performance indicators and the use of a multi tournament decision (MTD) method to extract the desired solutions. Furthermore, the design variables of each extracted solution, including its optimized topology, are provided.

Keywords Multi-objective truss structural optimization · Multi-objective evolutionary algorithms · Natural frequencies of vibration · Cardinality constraints · Automatic member grouping

1 Introduction

Recent advances in structural engineering, combined with the development of computational resources and techniques, have allowed the configuration of more complex structural projects that represent the modeling of a structure closest to its real behavior. It is common for designers to search for light and economic structures that meet safety criteria, which leads to constraints such as maximum displacements and stresses, as well as minimum values for natural frequencies

✉ Érica C. R. Carvalho
ericacrcarvalho@gmail.com

José Pedro G. Carvalho
jose.carvalho@engenharia.ufjf.br

Heder S. Bernardino
heder@ice.ufjf.br

Afonso C. C. Lemonge
afonso.lemonge@ufjf.br

Patrícia H. Hallak
patricia.hallak@engenharia.ufjf.br

Dênis E. C. Vargas
denis.vargas@cefetmg.br

[1] Graduate Program of Computational Modeling, Federal University of Juiz de Fora, Juiz de Fora, Brazil

[2] Civil Engineering Program, COPPE/Federal University of Rio de Janeiro, Rio de Janeiro, Brazil

[3] Department of Computer Science, Institute of Exact Sciences, Federal University of Juiz de Fora, Juiz de Fora, Brazil

[4] Department of Applied and Computational Mechanics, School of Engineering, Federal University of Juiz de Fora, Juiz de Fora, Brazil

[5] Department of Mathematics, Federal Center for Technological Education of Minas Gerais, Belo Horizonte, Brazil

of vibration, among others. Finding the optimal design with these conflicting objectives and constraints is a process of trial and error that is often too expensive and inefficient. The formulation of structural optimization problems is the most effective alternative. This formulation may contain one (single-objective) or more objectives (multi-objective) and several constraints: minimizing the weight of a structure and maximizing the first natural frequency of vibration (conflicting objectives), limiting stresses, identifying critical buckling loads, etc. This leads to a multi-objective formulation of a structural optimization problem.

Multi-objective structural optimization problems (MOSOPs) are of great interest in the optimization field. According to a table extracted from Lemonge et al. [49], and adapted and updated here as Table 1, the usual formulations for truss structures related MOSOPs generally consider minimizing weight and minimizing the maximum nodal displacements, subject to a set of several constraints. In contrast, in this paper, the problem of the structural optimization of trusses is formulated by considering minimizing the weight and maximizing the first natural frequency of vibration. Maximizing this frequency of vibration can ensure that resonance problems are avoided by "eliminating" the possibility of low-frequency excitations that can lead to the collapse of the structure. Furthermore, the importance of considering the dynamic behavior of structures should be highlighted, especially those submitted to structural optimization. In addition, a structure must be monitored throughout its useful life, maintaining its health and structural integrity, which can be directly affected by undesirable dynamic actions. This topic is addressed, for example, in [59, 75, 77, 92]. Reference [62], presented a discussion about structural optimization in civil engineering The authors provided an analysis of the optimization objectives and their temporal and spatial trends, and the optimization process.

Meta-heuristics are widely used to solve optimization problems, such as MOSOPs. They are an efficient method because they can be robust and free of derivatives of objective functions and constraints, making them increasingly popular in scientific fields and engineering. Among them are evolutionary algorithms (EAs) based on natural processes, commonly characterized by the presence of artificial mechanisms inspired by biology, such as reproduction, mutation, etc. Different kinds of meta-heuristics and EAs have been formulated in recent years. Some of the most widespread are the genetic algorithm (GA) [32], particle swarm optimization (PSO) [18], differential evolution (DE) [79], and ant colony optimization (ACO) [14], among others. Recently, some other meta-heuristics have been proposed. For example, Hayyolalam and Kazem [28] proposed a black widow optimization (BWO) algorithm inspired by the unique mating behavior of black widow spiders, while Patil and Kulkarni [70] proposed a novel multi-objective cohort intelligence (MOCI) algorithm based on Pareto dominance and coevolutionary design principles to achieve efficient, effective, productive, and robust performance. The capability of the MOCI algorithm is enhanced through the use of multiple features for the balance of exploration versus exploitation, search toward the promising region, and avoidance of search stagnation. Połap and Woźniak [71], proposed a mathematical model of red fox habits, including searching for food, hunting, and developing population while escaping from hunters, called the red fox optimization (RFO) algorithm. These proposals were subjected to benchmark tests and compared to other meta-heuristic algorithms to show potential advantages.

The meta-heuristics used to solve the problems formulated in this paper are the generalized differential evolution 3 (GDE3) [46], the nondominated sorting genetic algorithm II (NSGA-II) [15], the decision space-based niching (DN-NSGA-II) [53], the competitive mechanism-based multi-objective particle swarm optimizer (CMOPSO) [95], and the MOPSO with multiple search strategies (MMOPSO) [54]. These algorithms have their peculiarities and are able to provide a good basis for comparison concerning their performance. They were chosen for their popularity and efficiency, and are briefly described further in this text.

The structural sizing optimization (e.g., cross-sectional ares of the bars as design variables) is formulated in the MOSOPs presented in this paper. The sizing design variables are the cross-sectional areas of bars, which can be continuous or discrete. One difficult task is linking the bars automatically into a maximum number of groups established according to the designer's criteria. This grouping can provide economies in the cutting, transportation, assembly, welding, checking, etc., of the bars, as well as simplify the construction process [3, 10]. Cardinality constraints are applied to alleviate the designer of the task from needing to discover the best member grouping. Angelo et al. [1] proposed ant colony algorithms to solve of plane and spatial trusses with two conflicting objectives, minimizing the weight and the maximum nodal displacement. The authors also used cardinality constraints to find the optimal groupings of the bars and a decision-maker strategy to extract the desired solutions from the Pareto sets.

This paper's main contributions are to propose, formulate, and solve MOSOPs related to minimizing the total weight and maximizing the natural frequencies of vibrations of plane and spatial trusses. An automatic variable linking is used to find the best member groupings of bars according to the designer's preferences. The computational experiments are based on benchmark single-objective structural optimization problems widely discussed in the literature: the 10-, 25-, 72-, and 200-bar trusses. Five meta-heuristics are used

Table 1 Synthesis of related work concerning structural multi-objective problems in the context of this paper (adapted from Lemonge et al. [49] and updated here). W is the total weight or mass (in some cases), f_1 is the first natural frequency of vibration, u is the maximum displacement, λ^m is the buckling constraint for member m of the structure, σ is the allowable stress, and NCST is the number of different cross-section types. FRF is the frequency response function; $\overline{\text{FRF}}$ is the mean value of the FRF crest parameters concerning the natural frequencies of vibration f_1, f_2, and f_3; FT is the force transmissibility crest parameter with respect to f_i; $\overline{\text{FT}}$ is the mean value of FT crest parameters at f_1, f_2, and f_3; CMA is the constrained mass average; SDCV is the standard deviation of the constraints' violation; RI is the reliability index with RC reliability constraints; TPE is the total potential energy; LCC means life-cycle costs; GC refers to geometric constraints; and λ_1 is the first load factor concerning the elastic critical load (global stability)

References	Domain	Type	Objective functions	Constraint(s)	Algorithm(s)
[27]	2D	Frame	W, NCST	σ, λ^m, u	SPEA2, NSGA-II
[65]	2D	Truss bridge	$W, 1/f_1$	σ	PAES, NSGA-II, SPEA2, PBIL, MPSO
	3D	Walking tractor	$W, 1/\sum_{i=1}^{3}(f_1)$		
	2D	Truss bridge	W, FRF(f_1)		
			W, $\overline{\text{FRF}}$		
			W, $FT(F_1)$		
			W, $\overline{\text{FT}}$		
[25]	2D	Frame	CMA, SDCV	σ, λ^m, u	NSGA-II, SPEA2
[66]	3D	Truss tower	M, $1/\sum_{i=1}^{3}(F_i u_i)$	σ	SPEA2, PBIL, AMOSA
[81]	2D	Truss	W, u	σ	AMISS-MOP
[73]	2D-3D	Truss	W, u	σ	KSR
			W, f_1	σ, λ^m, u	
[26]	2D	Truss	W, RI	RC	CoSAR
			W, $f_1+f_2+f_3$	λ^m	
			$W, 1/\sum_{i=1}^{3} FRF(f_i)$	ad hoc	
			$W, 1/\sum_{i=1}^{3} FT(f_i)$		
[39]	2D-3D	Truss	W, u	σ	gM-PAES
[24]	2D-3D	Truss	W, u	σ	MO-CLFBA, MO-FA
[41]	2D-3D	Truss	W, u	σ	CSS
[33]	2D	Truss	W, u	σ	MOPSO
[1]	2D-3D	Truss	W, u	σ	MOAS, MOACS
[90]	2D-3D	Truss	W, u	σ	AICSAMO
[83]	2D-3D	Truss	W, u	σ	MOASOS
[64]	2D-3D	Truss	W, u, f_1, TPE	σ	FC-MOPSO
			W, u, f_1	σ, u	
			W, u	σ	
[63]	2D	Frame	W, $LCCs$	GC, PH	Surrogate FC-MOPSO
[86]	2D-3D	Truss	W, u	σ	GDE3, GDE3+APM NSGA-II
[40]	2D-3D	Truss	W, u	σ	MOCBO
[38]	2D-3D	Truss	W, u	σ	MOVPS, MOCBO
[84]	2D-3D	Truss	W, u	σ	MOMASOS
[2]	2D-3D	Truss	W, u	σ	MSOGP
[47]	2D-3D	Truss	W, u	σ	MOMHTS
[89]	2D	Truss	W, u	σ	SLDM-NSGA-II
[49]	2D-3D	Truss	W, f_1	σ, λ_1, u	GDE3
			W, λ_1	σ, f_1, u	
			W, u	σ, λ_1, f_1	
[9]	2D-3D	Truss	W,f_1, u	σ, λ_1	GDE3, SHAMODE, SHAMODE-WO, MM-IPDE
			W, λ_1, u	σ, f_1	
			W, f_1, λ_1	σ, u	
			W, f_1, u, λ_1	σ	
[87]	2D-3D	Truss	W, u	σ	User preference oriented R-GDE3, R-GDE3+APM R-NSGA-II
[82]	2D-3D	Truss	W, u	σ	MOHTS
[20]	2D-3D	Truss	Mass, Compliance	σ, u	MOWCA, MOEA/D NSGA-II , MODA MOSWCA

Table 1 (continued)

References	Domain	Type	Objective functions	Constraint(s)	Algorithm(s)
[43]	3D	Truss	W, u	σ	MOPSO, SPEA2 NSGA-II, MOTEO
[11]	2D-3D	Truss	W, u	σ	MOFBI and others
This study	2D-3D	Truss	W,f_1	σ, u	CMOPSO, DN-NSGA-II GDE3, MMOPSO NSGA-II

to solve these problems, and some performance analyses are considered.

This paper is organized as follows: Sect. 1.1 presents a literature review. Sect. 2 describes the formulation of the MOSOP discussed in this paper. The automatic member grouping and cardinality constraints are presented in Sect. 2.2. Sect. 3 presents the multi-objective evolutionary algorithms used in the experiments. Sect. 4 presents the performance indicators of the algorithms. Multicriteria decision making is discussed in Sect. 5 to define the preferred solutions to be extracted from the Pareto sets. Sect. 6 presents the computational experiments and the analysis of results, and finally, conclusions and extensions are considered in Section 7.

1.1 Literature review

Table 1, adapted from Lemonge et al. [49] and updated here, summarizes details of the domain (2D or 3D), the type of structure (truss, frame, bridge, etc.), the objective functions, the constraints, and the algorithm(s) outilined in the literature review in the context of this paper. The innovation that is emphasized between this paper and the propositions, discussions, approaches, and structural optimization problems mentioned in Table 1 is that they do not simultaneously consider the objectives, constraints, and automatic member grouping, which can be considered as one of the main objectives of this paper."

2 The multi-objective structural optimization problem

Although single-objective structural optimization problems are commonly found in the literature, the formulation of optimization problems involving multiple objectives appears naturally due to the presence of two or more conflicting objectives.

The MOSOP discussed in this paper is formulated as:

$$\begin{aligned} \min \quad & W(\mathbf{x}) \text{ and } \max \quad \omega_1(\mathbf{x}) \\ \text{s.t.} \quad & \sigma_i(\mathbf{x}) \le \overline{\sigma} \\ & u_j(\mathbf{x}) \le \overline{u} \\ & \mathbf{x}^L \le \mathbf{x} \le \mathbf{x}^U \end{aligned} \tag{1}$$

where $W(\mathbf{x})$ is the weight of the structure, $\omega_1(\mathbf{x})$ is the first natural frequency of vibration, $\sigma_i(\mathbf{x})$ is the axial stress at the i-th bar, and $u_j(\mathbf{x})$ is the displacement at the j-th node. The design variables are $\mathbf{x} = \{A_1, A_2, ..., A_N\}$, where A_i are the sizing design variables indicating the cross-sectional areas of the N bars (continuous or discrete) that are in the lower $\mathbf{x}^L$ and upper $\mathbf{x}^U$ bounds. The numerical experiments discussed in this paper were inspired by the problems with a single-objective function (weight minimization) traditionally addressed in the literature. The constraints were kept unchanged as the axial stresses in the bars and nodal displacements. In this case, no additional constraints, such as those concerning a structure's global stability, were considered. The total weight $W(\mathbf{x})$ is written as:

$$W(\mathbf{x}) = \sum_{i=1}^{N} \rho A_i L_i, \tag{2}$$

where ρ is the specific mass of the material and L_i is the length of the i-th bar of the structure, and $\omega_1(\mathbf{x})$ is obtained by the evaluation of the eigenvalues of the matrix

$$\left[(\omega_{m_f}^2 \times [\mathbf{M}]) + [\mathbf{K}]\right] = 0, \tag{3}$$

where $[\mathbf{M}]$ is the mass matrix and ω_{m_f} are the equivalent eigenvalues with respect to the m_f natural frequencies of vibration of the structure [7].

2.1 Finite element analysis

The matrices $[\mathbf{K}]$ and $[\mathbf{M}]$ are assembled after transformation to a global axis with the element rotation matrix R_i for the i-th element, where K_i and M_i are the elemental stiffness and mass [7], by the equations:

$$[\mathbf{K}] = \sum_{i=1}^{N} \left[[R_i]^T [K_i] [R_i] \right], \tag{4}$$

$$[\mathbf{M}] = \sum_{i=1}^{N} \left[[R_i]^T [M_i] [R_i] \right]. \quad (5)$$

The nodal displacements $\{u_j(\mathbf{x})\}$ are obtained by the equilibrium equation for a discrete system of bars (truss finite element), which is written as:

$$[\mathbf{K}]\{u_j(\mathbf{x})\} = \{p\}, \quad (6)$$

where $\{p\}$ are the load components. After obtaining the nodal displacements, it is possible to determine the final actions at each member's end through matrix operations [7]. The natural frequencies of vibration are obtained by Eq. (3). The complete and detailed description of the finite element method can be obtained, for example, in [7, 34, 61].

2.2 Automatic member grouping and cardinality constraints

Automatic member grouping is a significant advantage when designing a structure. Benefits can be obtained in fabrication, checking, assembling, transportation, and welding, as well as labor-saving in the production process of the members during manufacturing. In general, these aspects are not explicitly included in the cost functions of the desirable structural configuration. Some related papers on this theme are reported here.

Barbosa et al. presented several papers on solving structural optimization problems considering single and multiple cardinality constraints [5, 6, 50, 51]. Herencia and Haftka [30, 31] proposed a genetic algorithm-gradient strategy to find the minimum weight of the well known 10-bar truss. Liu et al. [55] studied the optimum conceptual design of pile foundations at the initial design stage, and also presented a singular optimum topology of skeletal structures with frequency constraints in Liu et al. [56]. Strategies for the cost of beams in reinforced concrete buildings using cardinality constraints were presented by Kripka et al. [44, 45]. Angelo et al. [1] proposed an algorithm considering two ant colony optimization algorithms to tackle MOSOPs with cardinality constraints. The optimal design of dome structures with dynamic frequency constraints was discussed by Kaveh and Ghazaan [37] using a strategy based on cascading that reduced the objective function value over a number of optimization stages. Carvalho et al. [10] proposed a CRPSO algorithm to solve sizing structural optimization problems with multiple frequency constraints using cardinality constraints to find the best member groupings. Several sets of numerical experiments were analyzed, including large-scale problems. The experiments considered discrete sizing and shape design variables simultaneously. Their article also incorporated a more detailed literature review considering cardinality constraints to find the best member groupings of bars. Some basic steps in using cardinality constraints for optimal grouping of members are illustrated in the next subsection.

2.3 Design variable linking for the automatic member grouping

A designer may require, for instance, that at most a given m of distinct cross-sectional areas should be used in the whole structure, leading to the need to group all bars in only m groups. Thus, the optimization problem must consider additional constraints requiring that no more than m ($m \leq N$) different cross-sectional areas should be used, that is, $A_i \in C_m = \{S_1, S_2, \ldots, S_m\}$, $i = 1, 2, \ldots, N$, where the cross-sectional areas $S_j, j = 1, 2, \ldots, m$ are unknown but belong to a larger ($N > m$) given set $S = \{A_1, A_2, \ldots, A_N\}$. These additional constraints are defined as cardinality constraints, and the standard structural optimization problem (without set cardinality constraint) is recovered when $m = N$.

An example of encoding a particle with 12 design variables is presented in Fig. 1. This encoding is inspired by the chromosome proposed by Barbosa and Lemonge [5]. The cardinality constraints, for instance, $m = 2$, are represented by the two variables at the left part of the encoding. At the right part of the encoding, there are, in this illustration, 10 indices that point to the design variables of the left part. These indices point to a `table` with a given number of discrete values (cross-sectional areas of bars) that can be chosen. In this example, design variable 1 points to index 1, returning the value 0.5440, and design variable 2 points to index 18, returning 34.0000. On the right part of the encoding, for example, the fourth design variable points to the first design variable on the left part, and the bar referred to by this design variable has a cross-sectional area of 0.5440.

3 Multi-objective evolutionary algorithms

Multi-objective evolutionary algorithms (MOEAs) have attracted a lot of research effort during the last decades, and still form one of the most promising areas of research in the evolutionary computing [96]. Many studies dedicated to designing and implementing EAs to solve multi-objective optimization problems (MOPs) have shown excellent results in solving several problems.

The MOEAs used to solve the problems formulated in this paper are the nondominated sorting genetic algorithm II (NSGA-II) [15], the decision space-based niching (DN-NSGA-II) [53], the generalized differential evolution 3 (GDE3) [46], the competitive mechanism-based multi-objective particle swarm optimizer (CMOPSO) [95], and the MOPSO with multiple search strategies (MMOPSO) [54].

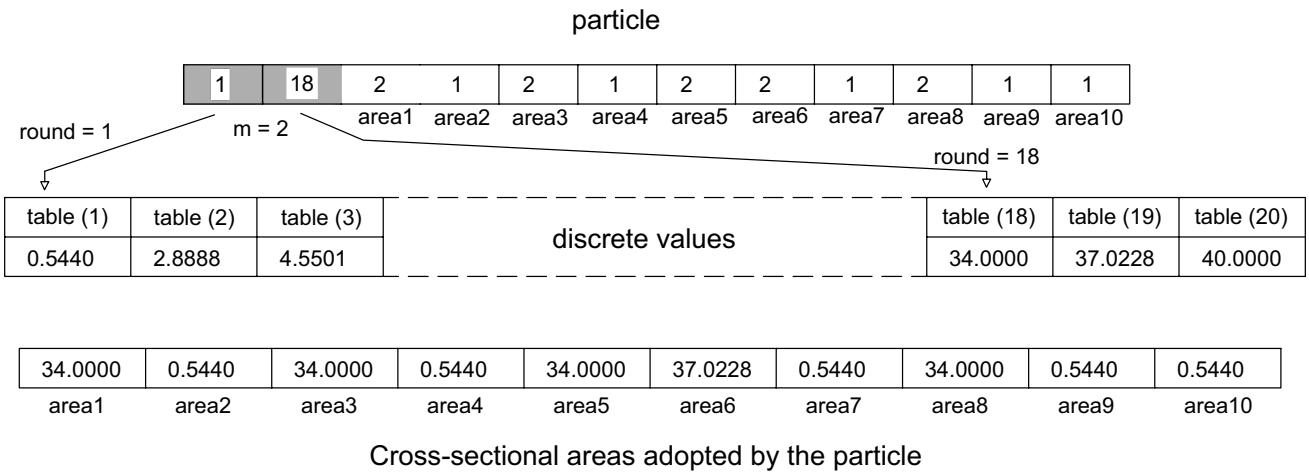

Fig. 1 Example of the encoding of a particle with 12 design variables. The cardinality constraints ($m = 2$) are represented by the two design variables at the left part of the vector that represents the particle. At the right part of the vector there are, for instance, 10 indices that point to the design variables at the left part

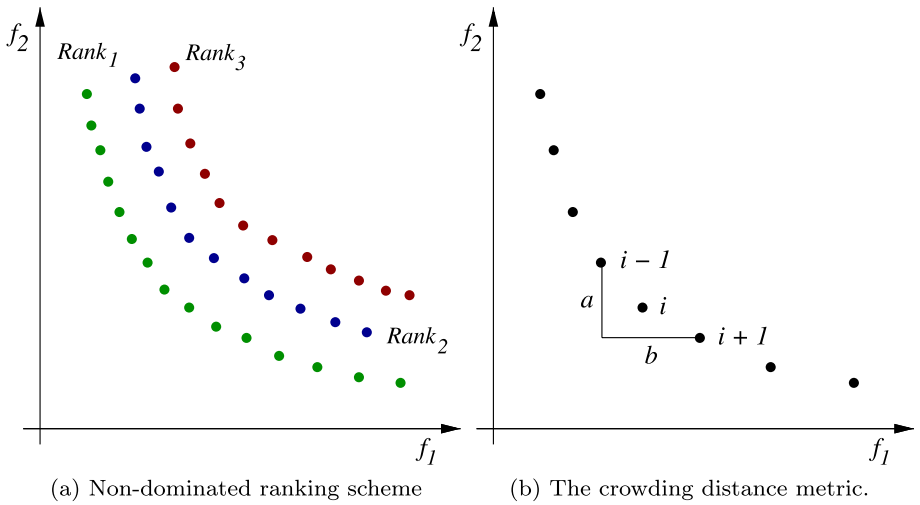

(a) Non-dominated ranking scheme (b) The crowding distance metric.

Fig. 2 Illustrations of 2**a** non-dominated ranking and 2**b** crowding distance, extract from [87]. The crowding distance value for solution i is equal to $a + b$

They were chosen for their popularity and efficiency, and are briefly described below.

NSGA-II is one of the most popular MOEAs, with three special characteristics: a fast non-dominated sorting approach (non-dominated ranking scheme), a fast crowding distance estimation procedure (crowding distance (CD) measure), and a simple crowding comparison operator. The non-dominated ranking scheme defines the non-domination levels, while the CD measures the solutions' diversity.

In NSGA-II, both parent and offspring populations are merged, and the non-dominated ranking scheme is executed. The solutions from the best ranks are picked to form the next population generation. CD is applied to calculate the local density of points in the objective space to select solutions with the same rank level. The idea is to sum the differences between the objective function values of the nearest neighbors according to each objective. An infinite CD value is given to the individuals at the boundary of each front rank level. Solutions with the biggest CD values are favored, contributing to better diversity. NSGA-II decreases the population's size using the non-dominated ranking and CD methods illustrated in Fig. 2a, b.

The NSGA-II version for continuous space variables commonly uses the well-known simulated binary crossover operator (SBX) for crossover and mutation of the population's individuals. Several works use NSGA-II (or some variation of it) applied in various MOSOPs [11, 25, 27, 42, 43, 65, 67, 86, 87, 89].

DN-NSGA-II is a modification of NSGA-II, and uses a crowding method in decision space as a niching technique for mating selection. The goal is to maintain different solutions corresponding to the same Pareto front point since, in practical applications, some MOPs have different Pareto sets with the same objective values. Applications that use the DN-NSGA-II algorithm can be found in [57, 60, 68, 91]. However, no application of the DN-NSGA-II in MOSOPs was found in the literature. As far as we know, the present work applies them in this context for the first time.

GDE3 extended differential evolution [78, 80] for constrained MOPs. For each candidate solution vector $\mathbf{x}$, three distinct vectors, $\mathbf{x}_{r_1}$, $\mathbf{x}_{r_2}$, and $\mathbf{x}_{r_3}$ (all different from $\mathbf{x}$) are randomly selected in the population. Then, the following well-known DE/Rand/1/Bin scheme is applied to create a vector $\mathbf{v} = \mathbf{x}_{r_1} + F(\mathbf{x}_{r_2} - \mathbf{x}_{r_3})$, where F is a user-defined parameter (commonly set as 0.5). Depending on the crossover rate $CR \in [0, 1]$, a trial vector $\mathbf{u}$ is created from a combination of vectors $\mathbf{v}$ and $\mathbf{x}$. After, $\mathbf{u}$ is compared to $\mathbf{x}$ using a constraint domination concept. As a result, $\mathbf{u}$ is selected to replace $\mathbf{x}$ in the next generation if $\mathbf{u}$ constraint dominates $\mathbf{x}$. But if $\mathbf{x}$ constraint dominates $\mathbf{u}$, $\mathbf{u}$ is discarded, and $\mathbf{x}$ remains in the population. Otherwise, both are included in the population, which is reduced using the non-dominated ranking scheme and crowding distance measure. Works can be found in the literature in which GDE3 is applied to problems related to the design of truss structures [9, 49, 86, 87].

CMOPSO is a variant of PSO [18] algorithm and uses a competition-mechanism-based learning strategy designed to guide the search of PSO for multi-objective optimization. While in practice the performance of most existing PSO-based MOEAs depends on the global or personal best particles stored in an external archive, in the CMOPSO, the particles are updated based on the pairwise competitions performed in the current swarm at each generation. This pairwise competition is based on the angle between particle p to be updated and two randomly selected competitors a and b from the elite particle set. Let θ_1 and θ_2 be the angles between p and a and between p and b, respectively. The particle corresponding to the smallest angle wins the competition. For example, if $\theta_1 < \theta_2$, a wins the competition. Some applications are found in [16, 29, 95].

MMOPSO uses multiple search strategies in which a decomposition approach is adopted to decompose MOPs into a set of single-objective optimization problems (SOPs) and then each particle is assigned to optimize each SOP. Two search strategies for updating the particle's velocity are designed to accelerate the convergence speed and maintain population diversity, respectively. Jha et al. [36] and Zhang et al. [94] applied the MMOPSO algorithm to solve different types of problems.

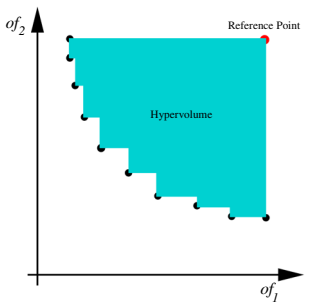

Fig. 3 In 2D, the HV is the area of the polygon whose vertices are the points of the optimal Pareto solutions and a reference point, extracted from Lemonge et al. [49]

4 MOEA performance

Most performance indicators evaluate the quality of an objective vector set in terms of at least one of the three criteria (the convergence, the uniformity, and the spread) [52]. In this study, the hypervolume (HV), the modified inverted generational distance (IGD+), the spacing (S), and the empirical attainment function (EAF) indicators are used to evaluate the performance of the algorithms. In addition, a tool for benchmarking and comparison optimization software that combines the best features of other tools for performance evaluation, called a performance profile, will be used. All metrics were chosen due to their popularity, and are described below in more detail.

4.1 Hypervolume

Hypervolume (HV) was proposed by Zitzler and Thiele [97], and is a performance indicator quite popular in the literature because it does not require knowledge of the real Pareto front of the problem in question. It is a unary indicator that assesses both the convergence and the diversity of solutions. As its name implies, it provides the hypervolume of the space limited by the points of the optimal Pareto solutions and a reference point.

In the case of two objective functions, hypervolume is the polygon area whose vertices are the points of the optimal Pareto solutions and a reference point. In Fig. 3, HV is the area hatched in blue, and the optimal Pareto solutions are the dots in red. The higher the HV value, the better the convergence/diversity ratio of the optimal Pareto solutions concerning the problem's real Pareto front.

4.2 IGD+

Let $A = \{a_1, a_2, \ldots, a_{|A|}\}$ the points found by a MOEA and $Z = \{z_1, z_2, \ldots, z_{|Z|}\}$ the reference points set (Pareto-front). The inverted generational distance (IGD) performance

indicator [13] evaluates the quality of A in terms of both convergence and diversity. The modified inverted generational distance (IGD+) indicator, proposed by Ishibuchi et al. [35], is weakly Pareto compliant, where the original IGD is not. Therefore, IGD+ is the average distance from each reference vector z to its nearest objective vector in the dominated region by A. Thus, IGD+ is calculated as follows:

$$\text{IGD+}(A) = \frac{1}{|Z|}\left(\sum_{z \in Z} \min_{a \in A} \left\{ \sqrt{\sum_{i=1}^{m} (\max\{a_i - z_i, 0\})^2} \right\} \right).$$

Small IGD+ values are preferable. The IGD+ evaluation demands that the true Pareto front be known, which does not generally happen. For these cases, Coello Coello et al. [12] suggests its approximation by non-dominated solutions obtained by all the algorithms together.

4.3 Spacing

The spacing (S) indicator was proposed by Schott [76], and numerically describes the spread of the Pareto front (PF) solutions. The S value is calculated through a relative Manhattan distance measure between each solution $s \in \text{PF}$ and the nearest PF solution different from it.

Given that n_{obj} is the number of objectives, $f_m(s)$ is the function value of the m-th objective at solution $s \in \text{PF}$, and the distance measure d_i is the minimum Manhattan distance between solution s_i and the others $s_k \neq s_i \in \text{PF}$, and $\bar{d}$ is the mean value of $d_i, i = 1, ..., |\text{PF}|$. Mathematically, S can be obtained by:

$$\text{S} = \sqrt{\frac{1}{|\text{PF}| - 1} \sum_{i=1}^{|\text{PF}|} (d_i - \bar{d})^2},$$

where

$$d_i = min\left\{ \sum_{m=1}^{n_{obj}} |f_m(s_i) - f_h(s_k)|, \forall s_k \neq s_i \in \text{PF} \right\}.$$

Thus, S is the standard deviation of the Manhattan distances from the PF. The value of the S indicator is smaller when the PF solutions are more evenly distributed. Therefore, smaller S values are preferable.

4.4 Empirical attainment function

The EAF, proposed by Fonseca and Fleming [21], operates as a measure of a probability distribution of the results obtained by an algorithm in the field of objectives. EAF is a summary of the results of several executions of an algorithm and, at the same time, allows for detecting if and where one algorithm is better than another. A discussion of how to obtain the EAF curve is given by [12, 21].

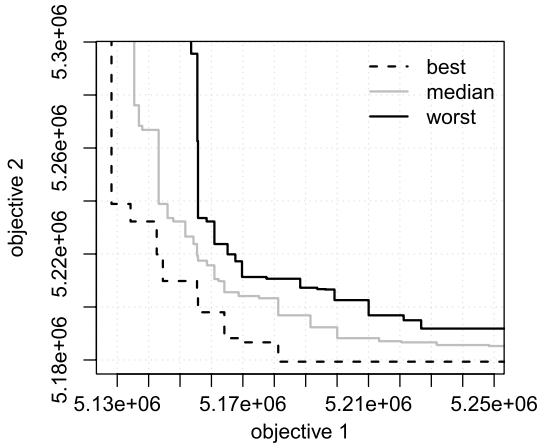

Fig. 4 Example of an EAF graph (best, median, and worst), taken from López-Ibánez et al. [58]

An example can be seen in Fig. 4, which displays an EAF graph (best, median, and worst curves) obtained by ten independent runs of a given MOEA on a problem with two objective functions to be minimized. Analyzing the figure, it is possible to observe that any solution obtained by any of these ten independent runs of the algorithm has a 0% chance of dominating some of the points of the best curve, a 50% chance of being dominated by some the median curve points, and a 0% chance of being dominated by any of the worst curve points.

4.5 Performance profiles

A distribution function for a performance metric and called a performance profile (PP) was introduced by Dolan and More [17]. Consider P a set of n_p problems, $\mathcal{S}$ a set of algorithms, and $t_{p,s}$ any indicator one wants to minimize, evaluated in problem p by algorithm s. The performance ratio is defined as

$$r_{p,s} = \frac{t_{p,s}}{min\{t_{p,s}, s \in \mathcal{S}\}}. \tag{7}$$

The performance profile $\rho_s(\tau)$ is defined as the probability that the performance ratio $r_{p,s}$ of algorithm $s \in \mathcal{S}$ is within a factor $\tau \geq 1$ of the best possible ratio. That is,

$$\rho_s(\tau) = \frac{1}{n_p} |\{p \in P : r_{p,s} \leq \tau\}|. \tag{8}$$

For any given algorithm s, the performance profile plot for each value of a positive factor τ is the percentage of problems from a given problem set in which s's performance is

within a factor of τ of the best performance of any algorithm on this problem. Barbosa et al. [4] indicated that the area under the performance profile curves is an overall performance indicator for an algorithm in a problem set. Larger values indicate higher solver efficiency in general.

5 Multicriteria decision making

The extraction of a solution from the Pareto fronts, which not only provides the values of the objective functions, but also the final values of the design variables, is of great interest to structural designers. Thus, the decision maker (DM) has a nontrivial task concerning how to select the solutions from the final non-dominated solutions. One way to do this, for example, is by defining a preference interval, which can provide a possibility to guide the DM preferences for exploring this range of solutions in a new multi-objective analysis.

In contrast, adopting preference weights (importance) for each of the objectives can build scenarios able to provide comparisons [1, 69]. However, this may not be a trivial task [93]. However, it is possible to use a strategy called multicriteria decision making (MCDM) that can indicate the preferred solutions from the weights defined by the DM. This strategy is adopted here to illustrate different scenarios defined by the DM to extract solutions from the Pareto fronts.

The MCDM establishes a MTD method, which is a tournament-based method that ranks the best and the worst possible solutions in the Pareto fronts, according to their objectives and preferences (weights) as established by the DM.

A function $R(a)$ is introduced and returns a global indicator or the preference for solution a when compared with others in the non-dominated solutions. It is necessary to give a criterion C defined by the DM, and each solution is compared to the other ones in the Pareto front. After that, a tournament function $T_i(a, AB)$ is adopted. This function returns the number of times that solution a wins the tournament when compared with another solution b, where AB is the whole set of solutions of the Pareto set. The function $T_i(a, AB)$ is written as:

$$T_i(a, AB) = \sum_{\forall b \in AB, a \neq b} \frac{td_i(a, b)}{(|AB| - 1)}, \tag{9}$$

where $td_i(a, b)$ is given by:

$$td_i(a, b) = \begin{cases} 1, \text{ if } f_i(b) - f_i(a) > 0, \\ 0, \text{ otherwise.} \end{cases} \tag{10}$$

At the end of the tournament, each solution has performance indicators, such as the scores provided by the function $T_i(a, AB)$, which inform its performance compared to the other solutions of set AB. These scores are aggregated in the global function ranking $R(\cdot)$, considering all the criteria and their respective weights w_i [93], where:

$$R(a) = \left(\prod_{i=1}^{no} T_i(a, AB)^{w_i} \right)^{1/no}. \tag{11}$$

The values for each weight w_i must be set by the DM according to the weight's importance, where $w_i \geq 0$ for $i = 1, \cdots, no$, and $\sum_{i=1}^{no} w_i = 1$. The scores defined by $R(a)$ provide a measure of the preference for a solution a in comparison with a solution b, such as:

- if $R(a) > R(b)$, then a is preferred to b;
- if $R(a) = R(b)$, then a is indifferent compared to b.

A pseudocode for this tournament-based method presented by Parreiras and Vasconcelos [69] is reproduced in Algorithm 1. Other techniques for extracting solutions from Pareto curves are found in the literature such as, for instance, AHP [74], Promethee II [8] and Smarts [19]. However, the goal here is not to conduct comparative studies between them. Details on the strengths and weaknesses of each of them can be found in these references or in Parreiras and Vasconcelos [69].

Algorithm 1: MTD pseudocode.

```
Initialize R as a vector filled only with ones and win as a matrix filled only with zeros;
for each alternative a ∈ AB do
    for each criterion c_i ∈ C do
        for each alternative b ∈ AB do
            d = f_i(b) − f_i(a);
            if d < 0 then
                win(a, c_i) = win(a, c_i) + 1 (a is preferred to b);
                else
                win(b, c_i) = win(b, c_i) + 1 (b is preferred to a);
            end
        end
    end
    R(a) = min{win(a, c_1)^{w_1}, ..., win(a, c_m)^{w_m}};
end
```

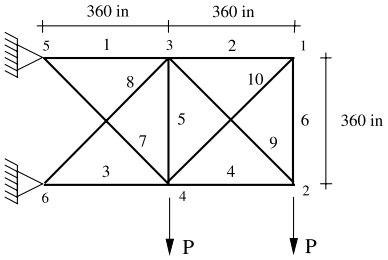

Fig. 5 10-bar truss, taken from Lemonge and Barbosa [48]

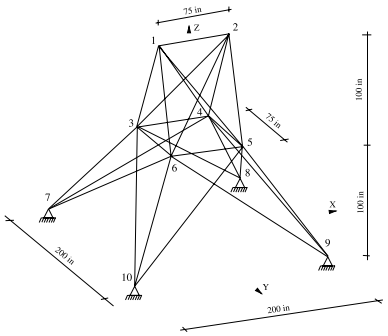

Fig. 6 25-bar truss, taken from Lemonge and Barbosa [48]

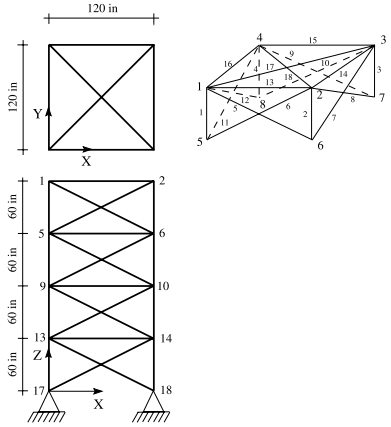

Fig. 7 72-bar truss, taken from Lemonge and Barbosa [48]

6 Computational experiments

This section assesses the performance of GDE3, NSGA-II, DN-NSGA-II, CMOPSO, and MMOPSO in constrained and unconstrained multi-objective optimization problems. Some constrained multi-objective optimization problems of planar and spatial truss structures are evaluated. In all experiments,

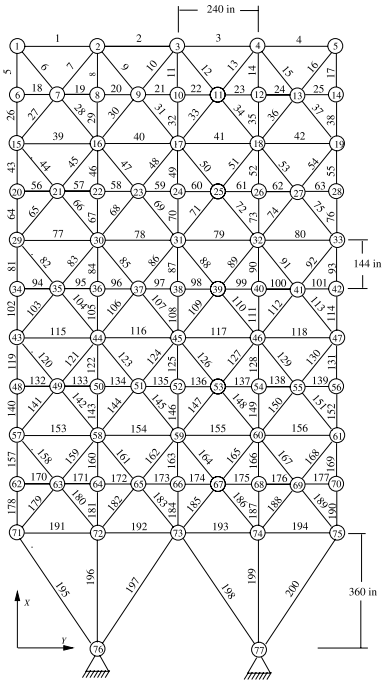

Fig. 8 200-bar truss, taken from Barbosa et al. [6]

Table 2 Some data of the structural optimization problems, where *ndv* is the number of decision variables, while nc_s and nc_d are the number of constraints concerning stress and displacements, respectively

Problem	References	*ndv*	nc_s	nc_d
10-Bar truss	[22]	10	10	8
25-Bar truss	[72]	8	25	18
72-Bar truss	[88]	16	144	96
200-Bar truss	[23]	29	600	–

the maximum number of objective function evaluations is 50000 , while the number of independent runs is 25 for the 10-, 25-, and 72-bar trusses, and 10 for the 200-bar truss. All of the presented solutions are rigorously feasible. Each experiment uses a randomly generated initial population.

Five algorithms provided in the PlatEMO platform [85] were adopted in this paper. The structures were analyzed by the finite element method (FEM) [34] during the evolutionary process. To obtain the HV was considering the maximum value for each coordinate from the union of all Pareto front points as a reference point. A tool developed by López-Ibánez et al. [58][1], was adopted to calculate and generate the EAF curves.

[1] http://lopez-ibanez.eu/eaftools

6.1 Structural multi-objective optimization problems

Four well-known MOSOPs, corresponding to the 10-, 25-, 72-, and 200-bar trusses, are analyzed and depicted in Figures 5,6, 78. In these problems, the first objective is to minimize the weight of the structure, and the second is to maximize the first natural frequency of vibration, considering stresses and/or displacements as constraints. Table 2 presents some data concerning these test-problems.

6.1.1 The 10-bar truss

In the 10-bar truss problem [22], the material has $\rho = 0.1$ lb/in^3 and E = 10^4 ksi. Vertical downward loads of 100 kips are applied at nodes 2 and 4, and the stress in each bar is limited *to* ± 25 ksi. In the discrete case, the values of the cross-sectional areas (in^2) are chosen from the set: 1.62, 1.80, 1.99, 2.13, 2.38, 2.62, 2.63, 2.88, 2.93, 3.09, 3.13, 3.38, 3.47, 3.55, 3.63, 3.84, 3.87, 3.88, 4.18, 4.22, 4.49, 4.59, 4.80, 4.97, 5.12, 5.74, 7.22, 7.97, 11.50, 13.50, 13.90, 14.20, 15.50, 16.00, 16.90, 18.80, 19.90, 22.00, 22.90, 26.50, 30.00, 33.50; this results in 42 options. For the continuous case, the lower and upper bounds for the cross-sectional areas are defined by [0.1; 40] (in^2). For the dynamic case, a non-structural mass of 1000 lb is attached to the free nodes, and displacement constraints are limited to 2 inches in the *x* and *y* directions.

6.1.2 The 25-bar truss

In the 25-bar truss problem [72], the material has $\rho = 0.1$ lb/in^3 and E = 10^4 ksi. The stress in each member is limited *to* ± 40 ksi. The values of the cross-sectional areas (in^2) are chosen from the set: 0.1, 0.2, 0.3, 0.4, 0.5, 0.6, 0.7, 0.8, 0.9, 1.0, 1.1, 1.2, 1.3, 1.4, 1.5, 1.6, 1.7, 1.8, 1.9, 2.0, 2.1, 2.2, 2.3, 2.4, 2.5, 2.6, 2.8, 3.0, 3.2, 3.4; this results in 30 options. For the continuous case, the lower and upper bounds of the cross-sectional areas are defined by [0.1; 3.4] (in^2). The loading data and the member grouping for the design variables, linked in eight groups, are detailed by Rajeev and Krishnamoorthy [72]. For the dynamic case, a non-structural mass of 100 lb is attached to nodes 1–2, and displacement constraints at the same nodes are limited to 0.35 inches in the *x* and *y* directions.

6.1.3 The 72-bar truss

In the 72-bar truss problem [88], the material has $\rho = 0.1$ lb/in^3 and E = 10^4 ksi, the stress in each member is limited *to* ± 25 ksi, and the values of the cross-sectional areas (in^2) are chosen from the set: $0.1, 0.2, 0.3, \ldots, 2.3, 2.4, 2.5$; this results in 25 options. For the continuous case, the lower and upper bounds of the cross-sectional areas are defined by [0.1; 2.5] (in^2). The loading data for this truss and the member grouping for the design variables, linked in sixteen groups, are detailed by Venkayya [88]. For the dynamic case, a non-structural mass of 5000 lb is attached to nodes 1–4, and displacement constraints are limited to 0.25 inches in the *x* and *y* directions.

6.1.4 The 200-bar truss

The 200-bar truss has the bars linked in 29 groups, as detailed by Ghasemi et al. [23]. The members have moduli elasticity and density equal to 30,000 ksi and 0.283 lb/in^3, respectively. The constraints imposed on the optimization problems are the stresses, which are limited *to* ± 10 ksi. Three load cases are considered: (1) 1.0 kip acting in the positive *x*–direction at nodes 1, 6, 15, 20, 29, 34, 43, 48, 57, 62, and 71; (2) 10 kips acting in the negative *y*–direction at nodes 1, 2, 3, 4, 5, 6, 8, 10, 12, 14, 15, 16, 17, 18, 19, 20, 22, 24,...,71, 72, 73, 74, and 75; and, finally, (3) the load cases (1) and (2) acting simultaneously. The lower and upper bounds of the cross-sectional areas (in^2) are defined by [0.1; 20] for the continuous case and are chosen from the set $\{0.1, 0.15, 0.2, 0.25, 0.3, ..., 20\}$ (in^2), for the discrete case, this results in 399 options. For the dynamic case, a non-structural mass of 220.458 lb is attached to nodes 1–5.

6.2 Results and discussions

The results obtained in all the experiments presented in this paper generate a significant number of Pareto curves. A comparative study of all these curves, one by one and being extensive, may not be conclusive. Accordingly, two analyses, considered more relevant, are presented in the following sections. The first analysis assesses the effect of using cardinality constraints through performance indicators in all analyzed structures, and the second one is performed to obtain the best solution according to MTD.

6.2.1 Analysis with cardinality constraints and performance indicators

The first analysis evaluates the effect of using cardinality constraints through performance indicators. The mean (M) and standard deviation (SD) values of the HV, IGD+, and spacing from all analyzed problems are shown in Tables 3 to 6, without set cardinality constraint and with $m = 2$, 4, 8 (if applicable), and 16 (if applicable), respectively. In Tables 3, 4, 5, and 6, the best results are highlighted in bold, and the (+) sign indicates that the difference between the measurements calculated for each of the runs performed is statistically significant (p-value ≤ 0.05) when compared to the

Table 3 Mean (M) and standard deviation (SD) of HV, IGD+, and S values obtained for all independent runs for the 10-Bar truss

		10-Bar truss (continuous)			10-Bar truss (discrete)		
Algorithm		HV	IGD+	S	HV	IGD+	S
$m = 0$							
CMOPSO	M	0.32786(+)	0.32106(+)	0.44221	**0.68855**	**0.00519**	0.00596(+)
	SD	0.05477	0.04739	0.50468	0.00112	0.00056	0.00299
DN-NSGA-II	M	0.86384(+)	0.00788(+)	0.00757(+)	0.48101(+)	0.21553(+)	0.00566(+)
	SD	0.02588	0.00232	0.00952	0.00603	0.00707	0.00079
GDE3	M	**0.90777**	**0.00200**	0.01449(+)	0.49199(+)	0.20503(+)	**0.00199**
	SD	0.00518	0.00022	0.01229	0.00347	0.00381	0.00022
MMOPSO	M	0.21832(+)	0.65616(+)	0.74550(+)	0.67830(+)	0.00828(+)	0.00940(+)
	SD	0.28956	0.40401	0.42971	0.00947	0.00174	0.00324
NSGA-II	M	0.87394(+)	0.00550(+)	**0.00473**	0.48147(+)	0.21658(+)	0.00248(+)
	SD	0.02849	0.00228	0.00353	0.00673	0.00747	0.00027
$m = 2$							
CMOPSO	M	0.64303	0.12612	0.00521(+)	0.32859(+)	0.32605(+)	0.06709(+)
	SD	0.02176	0.00633	0.00222	0.00001	0.00000	0.00438
DN-NSGA-II	M	0.63831(+)	0.13082(+)	0.00554(+)	0.30697(+)	0.34646(+)	0.03596(+)
	SD	0.02816	0.00458	0.00625	0.03633	0.04709	0.00877
GDE3	M	**0.66243**	0.12752	0.00391(+)	**0.33950**	**0.30492**	**0.02752**
	SD	0.03932	0.00819	0.00424	0.00290	0.00140	0.00459
MMOPSO	M	0.64549	**0.12560**	0.01413(+)	0.32828(+)	0.32643(+)	0.06913(+)
	SD	0.01845	0.00509	0.00353	0.00154	0.00189	0.00472
NSGA-II	M	0.64202(+)	0.12963(+)	**0.00335**	0.32147(+)	0.32767	0.03105(+)
	SD	0.02737	0.00407	0.00118	0.03152	0.04070	0.01089
$m = 4$							
CMOPSO	M	0.29898(+)	0.36641(+)	0.96016(+)	0.37156(+)	0.32383(+)	0.01746
	SD	0.10312	0.14297	0.19921	0.04124	0.04712	0.01309
DN-NSGA-II	M	0.81402(+)	0.03210(+)	0.00983(+)	0.45043(+)	0.24221(+)	0.01227(+)
	SD	0.04066	0.01196	0.01035	0.01631	0.01714	0.00312
GDE3	M	**0.85959**	**0.01785**	0.01080(+)	**0.46770**	**0.22623**	**0.00746**
	SD	0.02751	0.00435	0.01029	0.01380	0.01437	0.00126
MMOPSO	M	0.26576(+)	0.53350(+)	0.60312(+)	0.34169(+)	0.35812(+)	0.02593(+)
	SD	0.25248	0.36950	0.49619	0.04690	0.04937	0.01177
NSGA-II	M	0.82167(+)	0.03544(+)	**0.00529**	0.45683(+)	0.23402(+)	0.00828
	SD	0.04892	0.02054	0.00198	0.01350	0.01201	0.00227
$m = 8$							
CMOPSO	M	0.27074(+)	0.40350(+)	0.88000(+)	0.36760(+)	0.33596(+)	0.01037(+)
	SD	0.08321	0.18027	0.33166	0.03017	0.03107	0.00798
DN-NSGA-II	M	0.85191(+)	0.01221(+)	0.01064(+)	0.46299(+)	0.23241(+)	0.01350(+)
	SD	0.02948	0.00400	0.01118	0.01532	0.01637	0.00518
GDE3	M	**0.88135**	**0.00982**	0.01986(+)	0.47839	**0.21750**	0.00459(+)
	SD	0.01217	0.00263	0.01268	0.01764	0.01671	0.00157
MMOPSO	M	0.32142(+)	0.43256(+)	0.49009(+)	0.36761(+)	0.33493(+)	0.01241(+)
	SD	0.22857	0.33828	0.50040	0.02894	0.02930	0.00756
NSGA-II	M	0.86337	0.01122	**0.00502**	**0.47966**	0.21778	**0.00352**
	SD	0.04032	0.00418	0.00272	0.00884	0.01014	0.00101

The best results are highlighted in bold

same results obtained by the algorithm with the best mean, that is, the Wilcoxon test.

Considering the results from continuous and discrete cases of the 10-bar truss (Table 3), the GDE3 algorithm achieved the best results for all performance indicators. In

Table 4 Mean (M) and standard deviation (SD) of HV, IGD+, and S values obtained for all independent runs for the 25-bar truss

		25-Bar truss (continuous)			25-Bar truss (discrete)		
Algorithm		HV	IGD+	S	HV	IGD+	S
$m = 0$							
CMOPSO	M	**0.74713**	**0.00409**	0.00424(+)	**0.75278**	**0.00348**	0.00361(+)
	SD	0.00076	0.00034	0.00110	0.00068	0.00021	0.00082
DN-NSGA-II	M	0.51295(+)	0.09226(+)	0.00351(+)	0.52293(+)	0.10975(+)	0.00367(+)
	SD	0.00679	0.00248	0.00083	0.00662	0.00355	0.00069
GDE3	M	0.51865(+)	0.08932(+)	**0.00274**	0.52679(+)	0.10746(+)	0.00407
	SD	0.00718	0.00270	0.00186	0.00778	0.00412	0.00477
MMOPSO	M	0.74628(+)	0.00491(+)	0.00726(+)	0.75128(+)	0.00446(+)	0.00849(+)
	SD	0.00069	0.00038	0.00123	0.00069	0.00021	0.00284
NSGA-II	M	0.51708(+)	0.09011(+)	**0.00274**	0.52334(+)	0.10935(+)	**0.00277**
	SD	0.00548	0.00204	0.00065	0.00484	0.00262	0.00042
$m = 2$							
CMOPSO	M	**0.68131**	**0.05255**	0.00306(+)	**0.68599**	**0.05305**	**0.00896**
	SD	0.00210	0.00207	0.00030	0.00126	0.00052	0.00063
DN-NSGA-II	M	0.46421(+)	0.14017(+)	0.00587(+)	0.46970(+)	0.15448(+)	0.01507(+)
	SD	0.00973	0.00385	0.00167	0.01439	0.00807	0.00323
GDE3	M	0.47952(+)	0.13400(+)	**0.00128**	0.48435(+)	0.14647(+)	0.01355(+)
	SD	0.00071	0.00122	0.00016	0.00000	0.00000	0.00004
MMOPSO	M	0.67995(+)	0.05262(+)	0.00851(+)	0.68480(+)	0.05315(+)	0.01015(+)
	SD	0.00048	0.00027	0.00096	0.00036	0.00012	0.00070
NSGA-II	M	0.47866(+)	0.13409(+)	0.00368(+)	0.48435(+)	0.14647(+)	0.01354(+)
	SD	0.00155	0.00061	0.00032	0.00000	0.00000	0.00000
$m = 4$							
CMOPSO	M	0.74112	0.00668	**0.00372**	0.74619	**0.00688**	**0.00365**
	SD	0.00381	0.00202	0.00069	0.00338	0.00223	0.00136
DN-NSGA-II	M	0.50844(+)	0.09492(+)	0.00471(+)	0.50876(+)	0.11861(+)	0.01479(+)
	SD	0.01274	0.00484	0.00094	0.01774	0.00995	0.01754
GDE3	M	0.52113(+)	0.08908(+)	0.00612(+)	0.53121(+)	0.10555(+)	0.00996
	SD	0.00601	0.00299	0.01214	0.00423	0.00235	0.01613
MMOPSO	M	**0.74260**	**0.00587**	0.00874(+)	**0.74625**	**0.00688**	0.01039(+)
	SD	0.00140	0.00100	0.00129	0.00174	0.00091	0.00440
NSGA-II	M	0.51548(+)	0.09127(+)	0.00529(+)	0.52367(+)	0.10966(+)	0.01080(+)
	SD	0.01105	0.00433	0.01072	0.00853	0.00452	0.01554

The best results are highlighted in bold

specific analyses of the use or not of the cardinality constraint, with $m = 4$, the GDE3 algorithm was better in 83.33% of the indicators and with $m = 2$ in 66.66% of the indicators. However, Tables 4, 5, and 6 show that the best results were obtained by the CMOPSO algorithm for the 25-, 72-, and 200-bar trusses (for both continuous and discrete cases).

In Table 4, when no cardinality constraint was set and with $m = 2$, the CMOPSO was better in 66.66% and 83.33% of the indicators, respectively. For the 72-bar truss, when no cardinality constraint was set and with $m = 8$, the CMOPSO algorithm was better on 66.66% of the indicators. The CMOPSO did not obtain better results for the Spacing indicator. Finally, in Table 6, the CMOPSO algorithm was better on 66.66% of the indicators considering all cardinalities. However, it is important to highlight that in this table, the CMOPSO algorithm also did not obtain better results for the Spacing indicator.

Figures 9a, b, and c show the performance profile curves of the HV, IGD+, and spacing indicators, respectively. In each graph, the values in the caption indicate the areas under the curve, normalized by the largest of them, in this order: CMOPSO; DN-NSGA-II; GDE3; MMOPSO; NSGA-II. Fig. 9d shows the overall performance profile curves considering these areas as a global performance indicator.

These graphs support what was observed in the previous tables. For the HV and IGD+ indicators, the best result was obtained by the CMOPSO algorithm, followed by the

Table 5 Mean (M) and standard deviation (SD) of HV, IGD+, and S values obtained for all independent runs for the 72-bar truss

		72-Bar truss (continuous)			72-Bar truss (discrete)		
Algorithm		HV	IGD+	S	HV	IGD+	S
$m = 0$							
CMOPSO	M	**0.81388**	**0.00392**	0.00325(+)	**0.81585**	**0.00330**	0.00354(+)
	SD	0.00072	0.00027	0.00056	0.00069	0.00017	0.00116
DN-NSGA-II	M	0.75037(+)	0.01609(+)	0.00402(+)	0.75232(+)	0.02358(+)	0.00460(+)
	SD	0.00437	0.00097	0.00056	0.00485	0.00176	0.00068
GDE3	M	0.75975(+)	0.01090(+)	**0.00196**	0.76175(+)	0.01994(+)	**0.00196**
	SD	0.00425	0.00079	0.00037	0.00430	0.00172	0.00025
MMOPSO	M	0.81099(+)	0.00476(+)	0.00600(+)	0.81220(+)	0.00481(+)	0.00540(+)
	SD	0.00144	0.00038	0.00138	0.00189	0.00035	0.00065
NSGA-II	M	0.75667(+)	0.01220(+)	0.00303(+)	0.75988(+)	0.02050(+)	0.00300(+)
	SD	0.00481	0.00084	0.00028	0.00409	0.00158	0.00030
$m = 2$							
CMOPSO	M	**0.75593**	0.05608(+)	0.00359(+)	0.75301	0.05398	0.00695
	SD	0.00627	0.00674	0.00068	0.00243	0.00146	0.00379
DN-NSGA-II	M	0.69107(+)	0.06623(+)	0.01017(+)	0.68611(+)	0.07740(+)	0.01428(+)
	SD	0.00250	0.00131	0.00528	0.00824	0.00534	0.00423
GDE3	M	0.69544(+)	0.06457(+)	**0.00210**	0.69399(+)	0.07257(+)	0.00621(+)
	SD	0.00379	0.00085	0.00167	0.00196	0.00094	0.00050
MMOPSO	M	0.75587(+)	**0.05569**	0.00804(+)	**0.75324**	**0.05354**	0.00709(+)
	SD	0.00263	0.00310	0.00249	0.00206	0.00090	0.00251
NSGA-II	M	0.69594(+)	0.06443(+)	0.00446(+)	0.69274(+)	0.07301(+)	**0.00532**
	SD	0.00233	0.00049	0.00047	0.00358	0.00160	0.00083
$m = 4$							
CMOPSO	M	0.81238(+)	0.00435(+)	0.00349(+)	**0.81353**	**0.00439**	0.00356(+)
	SD	0.00585	0.00532	0.00096	0.00219	0.00175	0.00110
DN-NSGA-II	M	0.74882(+)	0.01903(+)	0.01017(+)	0.74317(+)	0.03188(+)	0.01539(+)
	SD	0.00621	0.00386	0.00223	0.00664	0.00416	0.00427
GDE3	M	0.75545(+)	0.01148(+)	**0.00228**	0.75576(+)	0.02254(+)	**0.00224**
	SD	0.00509	0.00092	0.00108	0.00555	0.00221	0.00084
MMOPSO	M	**0.81270**	**0.00378**	0.00737(+)	0.81279	0.00493(+)	0.00761(+)
	SD	0.00142	0.00112	0.00209	0.00208	0.00117	0.00274
NSGA-II	M	0.75822(+)	0.01137(+)	0.00425(+)	0.75770(+)	0.02235(+)	0.00411(+)
	SD	0.00473	0.00094	0.00035	0.00263	0.00135	0.00060
$m = 8$							
CMOPSO	M	**0.81359**	**0.00364**	0.00330(+)	**0.81595**	**0.00302**	0.00326(+)
	SD	0.00317	0.00301	0.00169	0.00100	0.00037	0.00102
DN-NSGA-II	M	0.75375(+)	0.01396(+)	0.00658(+)	0.74775(+)	0.02792(+)	0.01162(+)
	SD	0.00503	0.00126	0.00121	0.00762	0.00325	0.00324
GDE3	M	0.75398(+)	0.01174(+)	**0.00283**	0.75618(+)	0.02229(+)	**0.00249**
	SD	0.00619	0.00112	0.00194	0.00418	0.00171	0.00094
MMOPSO	M	0.81226(+)	0.00392(+)	0.00664(+)	0.81373(+)	0.00424(+)	0.00632(+)
	SD	0.00162	0.00059	0.00117	0.00102	0.00047	0.00084
NSGA-II	M	0.75995(+)	0.01101(+)	0.00387(+)	0.76200(+)	0.02014(+)	0.00371(+)
	SD	0.00389	0.00074	0.00034	0.00354	0.00131	0.00039

The best results are highlighted in bold

Table 6 Mean (M) and standard deviation (SD) of HV, IGD+, and S values obtained for all independent runs for the 200-bar truss

		200-Bar truss (continuous)			200-Bar truss (discrete)		
Algorithm		HV	IGD+	S	HV	IGD+	S
$m = 0$							
CMOPSO	M	**0.91555**	**0.00158**	0.00379(+)	**0.91652**	**0.00164**	0.00373(+)
	SD	0.00031	0.00018	0.00030	0.00026	0.00012	0.00032
DN-NSGA-II	M	0.65261(+)	0.17843(+)	0.00139(+)	0.65684(+)	0.17378(+)	0.00138(+)
	SD	0.00527	0.00434	0.00055	0.01072	0.00757	0.00034
GDE3	M	0.63448(+)	0.18924(+)	0.00301(+)	0.64052(+)	0.18463(+)	0.00374(+)
	SD	0.00854	0.00457	0.00083	0.01118	0.00826	0.00242
MMOPSO	M	0.86772(+)	0.01201(+)	0.00451(+)	0.85550(+)	0.01469(+)	0.00433(+)
	SD	0.03484	0.01035	0.00045	0.03969	0.01086	0.00054
NSGA-II	M	0.64869(+)	0.18073(+)	**0.00096**	0.66472(+)	0.16919(+)	**0.00101**
	SD	0.02514	0.01299	0.00024	0.00793	0.00670	0.00015
$m = 2$							
CMOPSO	M	**0.67245**	**0.12541**	0.00272(+)	**0.69853**	**0.11063**	0.00418(+)
	SD	0.04497	0.02321	0.00171	0.00495	0.00175	0.00315
DN-NSGA-II	M	0.25768(+)	0.51408(+)	0.00226(+)	0.26371(+)	0.50344(+)	0.00615(+)
	SD	0.03019	0.03646	0.00073	0.02678	0.03262	0.00502
GDE3	M	0.31062(+)	0.44822(+)	**0.00120**	0.31358(+)	0.44379(+)	**0.00083**
	SD	0.03055	0.03599	0.00121	0.02669	0.03655	0.00052
MMOPSO	M	0.63923	0.14032	0.00564(+)	0.65076(+)	0.13336(+)	0.00530(+)
	SD	0.07241	0.03751	0.00093	0.06920	0.03494	0.00074
NSGA-II	M	0.24271(+)	0.53187(+)	0.00128	0.24780(+)	0.52418(+)	0.00187(+)
	SD	0.03253	0.03837	0.00029	0.04159	0.04919	0.00113
$m = 4$							
CMOPSO	M	**0.83552**	**0.03476**	0.00290(+)	**0.84793**	**0.02884**	0.00329(+)
	SD	0.02465	0.01103	0.00038	0.01250	0.00574	0.00033
DN-NSGA-II	M	0.38442(+)	0.37663(+)	0.00186	0.41100(+)	0.35443(+)	0.00341(+)
	SD	0.04971	0.04550	0.00070	0.04284	0.03607	0.00089
GDE3	M	0.52143(+)	0.26862(+)	0.00246(+)	0.49958(+)	0.28620(+)	0.00333(+)
	SD	0.02819	0.02223	0.00088	0.03634	0.03256	0.00100
MMOPSO	M	0.76305(+)	0.06069(+)	0.00485(+)	0.72913(+)	0.07177(+)	0.00535(+)
	SD	0.04939	0.01953	0.00054	0.07229	0.02667	0.00400
NSGA-II	M	0.40313(+)	0.35893(+)	**0.00165**	0.43218(+)	0.33459(+)	**0.00125**
	SD	0.05656	0.04936	0.00092	0.03392	0.03083	0.00022
$m = 8$							
CMOPSO	M	**0.88451**	**0.01270**	0.00351(+)	**0.87848**	**0.01457**	0.00345(+)
	SD	0.01285	0.00455	0.00040	0.01248	0.00498	0.00038
DN-NSGA-II	M	0.49951(+)	0.28087(+)	0.00174(+)	0.50561(+)	0.27435(+)	0.00307(+)
	SD	0.04080	0.03029	0.00032	0.05161	0.03981	0.00140
GDE3	M	0.53517(+)	0.25558(+)	0.00498(+)	0.54294(+)	0.25064(+)	0.00485(+)
	SD	0.02194	0.01656	0.00146	0.03334	0.02578	0.00070
MMOPSO	M	0.72027(+)	0.07185(+)	0.00663(+)	0.71617(+)	0.07132(+)	0.00383(+)
	SD	0.07773	0.03645	0.00693	0.06901	0.03157	0.00072
NSGA-II	M	0.50489(+)	0.27786(+)	**0.00142**	0.51606(+)	0.26894(+)	**0.00153**
	SD	0.05484	0.04106	0.00049	0.03423	0.02581	0.00069
$m = 16$							
CMOPSO	M	**0.89345**	**0.00996**	0.00357(+)	**0.89062**	**0.01012**	0.00367(+)
	SD	0.00964	0.00396	0.00039	0.00794	0.00329	0.00043
DN-NSGA-II	M	0.60205(+)	0.20805(+)	0.00198(+)	0.57436(+)	0.22362(+)	0.00208(+)
	SD	0.03481	0.02199	0.00079	0.04018	0.02613	0.00061

Table 6 (continued)

		200-Bar truss (continuous)			200-Bar truss (discrete)		
Algorithm		HV	IGD+	S	HV	IGD+	S
GDE3	M	0.26731(+)	0.49612(+)	0.00963(+)	0.27533(+)	0.49258(+)	0.01024(+)
	SD	0.05574	0.06362	0.00193	0.06408	0.08263	0.00211
MMOPSO	M	0.76605(+)	0.05128(+)	0.00495(+)	0.77649(+)	0.04542(+)	0.00461(+)
	SD	0.03060	0.01259	0.00216	0.05658	0.02030	0.00130
NSGA-II	M	0.55318(+)	0.24594(+)	**0.00156**	0.58874(+)	0.21732(+)	**0.00117**
	SD	0.08309	0.06191	0.00115	0.04499	0.03003	0.00014

The best results are highlighted in bold

MMOPSO. For the spacing indicator, the NSGA-II algorithm obtained the best result, followed by the GDE3 algorithm. Furthermore, in the analysis of the overall performance of the indicators, the CMOPSO algorithm reached first place, followed by the NSGA-II.

A more detailed analysis for each truss is presented in Figs. 10, 11, 12 and 13 showing the performance profile curves of 10-, 25-, 72, and 200-bar trusses, respectively, without set cardinality constraints and with $m = 2$, 4, 8 (if applicable), and 16 (if applicable). In the caption, the values of the areas under the curve are presented, normalized by the largest of them, in this order: CMOPSO; DN-NSGA-II; GDE3; MMOPSO; NSGA-II.

Fig. 10 shows the continuous case of the 10-bar truss, and the NSGA-II algorithm obtained the highest value of the area under the curve, considering all cardinality constraints. For the continuous case, without set cardinality constraints and with $m = 2$, the CMOPSO algorithm was superior, and with $m = 4$ and 8, the NSGA-II algorithm remained higher.

For the 25-bar truss, the curves presented in Fig. 11 show that the CMOPSO and MMOPSO algorithms reached the best performance when all cardinalities were considered (in both continuous and discrete cases). The other three algorithms, DN-NSGA-II, GDE3, and NSGA-II, obtained similar results, which were distant from those obtained by CMOPSO and MMOPSO.

The results for the 72-bar truss (Fig. 12) show that for the continuous and discrete cases, the CMOPSO algorithm obtained the highest value of the areas under the curve, followed by the MMOPSO algorithm. Both algorithms obtained the highest value when considering the discrete case and with $m = 2$ and 4. In general, the DN-NSGA-II algorithm was the one that had the worst performance.

Finally, in this analysis of the graphs obtained by the 200-bar truss presented in Fig. 13, it is observed that again, the highest value was obtained by the CMOPSO algorithm, followed by the MMOPSO. The other three algorithms obtained worse and farther values.

6.2.2 Decision-maker preferences

The second analysis takes into account all the information obtained by the Pareto fronts for all algorithms. The next step is asking the DM to articulate his/her preferences. Using the MTD method provides one configuration for the 72-bar truss (discrete case) considering three decision scenarios and two criteria: (i) the weight of the structure and (ii) the first natural frequency of vibration of the structure.

The scenarios are described as follows:

- Scenario A: criterion (i) is more important than criterion (ii), i.e. $(w_1, w_2) = (0.7, 0.3)$.
- Scenario B: both criteria have the same importance, i.e. $(w_1, w_2) = (0.5, 0.5)$.
- Scenario C: criterion (ii) is more important than criterion (i), i.e. $(w_1, w_2) = (0.3, 0.7)$.

Among the non-dominated solutions for the 72-bar truss obtained by the CMOPSO, DN-NSGA-II, GDE3, MMOPSO, and NSGA-II algorithms without set cardinality constraints, with $m = 2$, 4, and 8, as presented in Figs. 14, 15, 16 and 17, respectively, where the square represent the solutions selected by the MTD method in each scenario. In addition, the optimized topology of each extracted solution is also depicted in these figures.

In Figs. 14b, 15b, 16b, and 17b, it is possible to observe that the solutions found by the MTD showed lower values for the weight and the first natural frequency of vibration compared to those shown in Figs. 14c and d, 15c and d, 16c and d, and 17c and d. This is expected behavior, as their respective importance $w_1 = 0.7$, is bigger than those used in scenarios B and C. In contrast, in scenario C, the importance $w_1 = 0.3$ is lower than those used in other scenarios, which results in solutions with higher values for the weight and for first natural frequency of vibration. For scenario B, which has the same values for w ($w_1 = w_2 = 0.5$), both objective function values are in the range of their respective values in scenarios A and C.

Additionally, the final values of each objective function and the design variables of the solutions found by

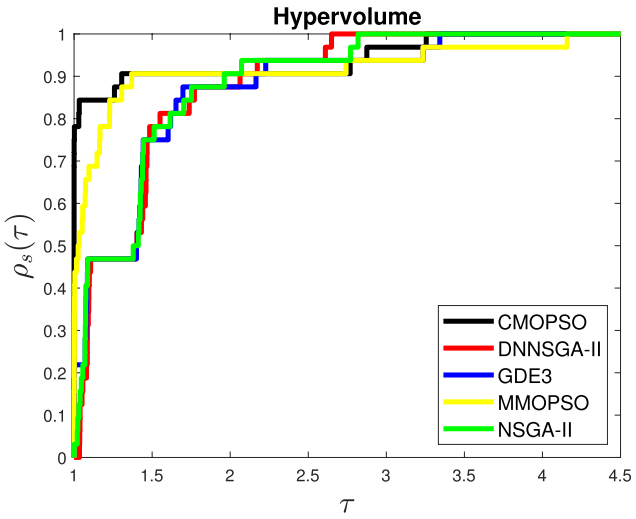

(a) 1; 0.93060; 0.92120; 0.97194; 0.93322.

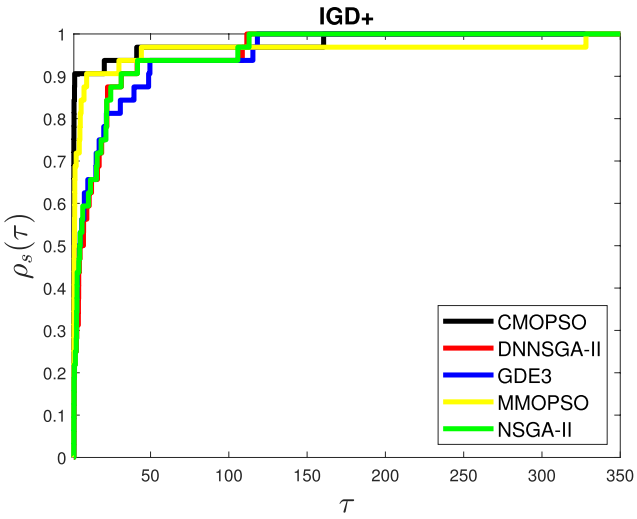

(b) 1; 0.97384; 0.97006; 0.97897; 0.97514.

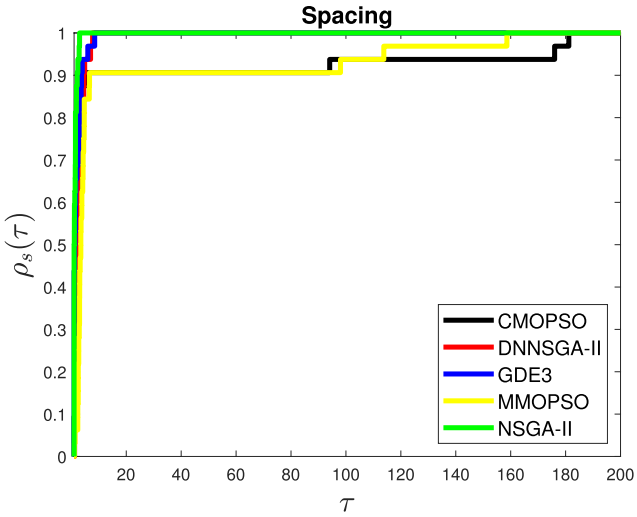

(c) 0.91834; 0.99296; 0.99602; 0.92563; 1.

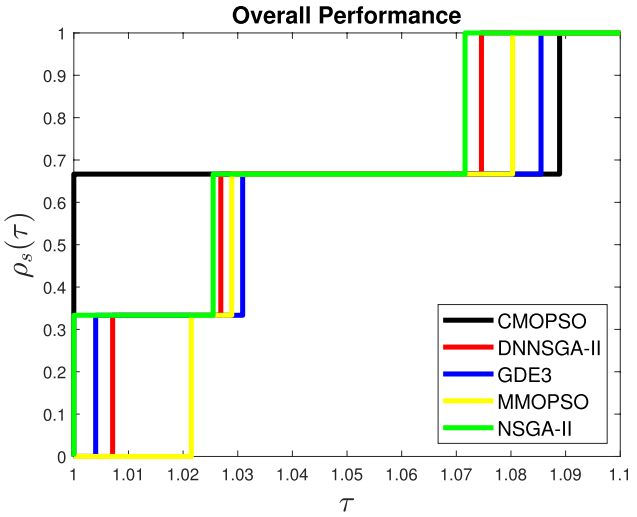

(d) 1; 0.88920; 0.82283; 0.76490; 0.95388.

Fig. 9 Performance profile curves of the indicators considered here: **a** Hypervolume, **b** IGD+, **c** Spacing, and **d** Overall performance. The values in each graph indicate the areas under the curve, normalized by the largest of them, in this order: CMOPSO; DN-NSGA-II; GDE3; MMOPSO; NSGA-II

the MTD method are provided in Table 7. The previously mentioned observations related to the results obtained by the 72-bar truss in the three scenarios analyzed through the figures can be confirmed with the values presented in this table.

7 Conclusions and extensions

Usually, in structural optimization problems, conflicting objectives, such as the mass and the maximum nodal displacement, are minimized in the context of framed structures, such as trusses. To avoid problems with resonance,

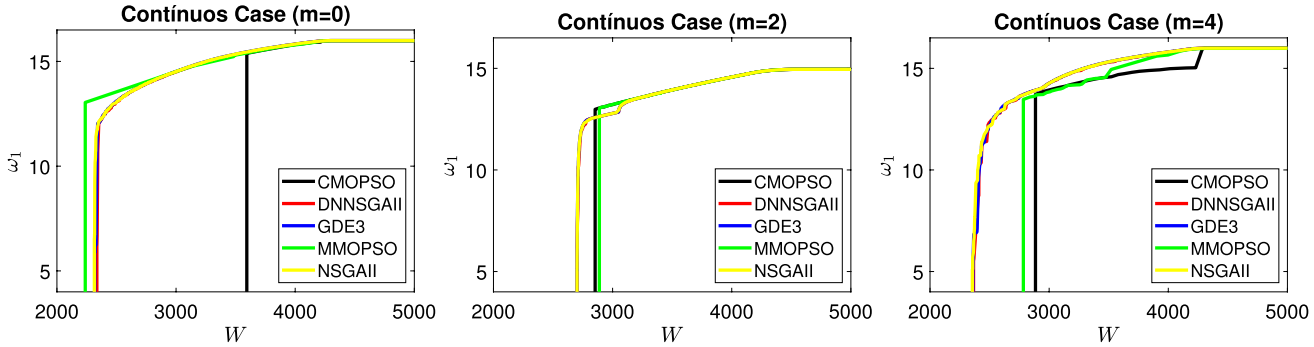

(a) 0.401; 0.991; 0.996; 0.995; 1. (b) 0.941; 0.998; 1; 0.924; 1. (c) 0.735; 0.991; 0.996; 0.801; 1.

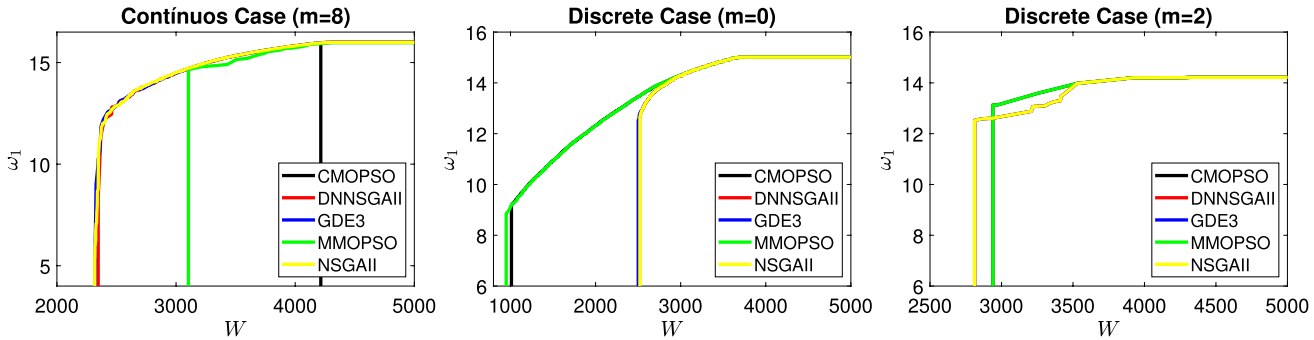

(d) 0.058; 0.993; 1; 0.650; 1. (e) 1; 0.614; 0.620; 0.999; 0.613. (f) 1; 0.871; 0.871; 1; 0.871.

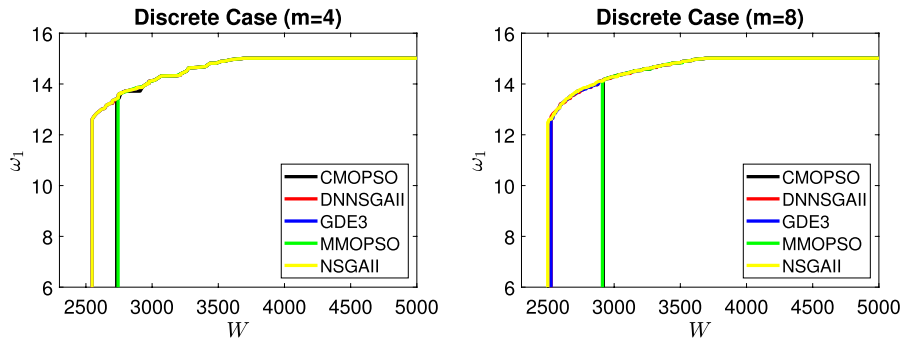

(g) 0.949; 0.999; 1; 0.941; 1. (h) 0.798; 0.990; 0.995; 0.803; 1.

Fig. 10 EAF_{best} solutions of the 10-bar truss. The values in each graph indicate the areas under the curve, normalized by the largest of them, in this order: CMOPSO; DN-NSGA-II; GDE3; MMOPSO; NSGA-II

which can lead to the collapse of structures, they can be designed by making the first natural frequency of vibration high. Furthermore, it is crucial to stay away from excitation frequencies. This problem is formulated as a multi-objective optimization problem, which is clearly an issue of great interest in structural engineering.

This paper proposed the formulation of a new multi-objective optimization problem in which the maximization of the first natural frequency of vibration is a conflicting objective function with the minimization of the structure's weight. Five multi-objective algorithms were used to solve those problems considering natural frequencies and additional cardinality constraints. The performance of this approach was evaluated on four structural multi-objective optimization problems: 10-, 25-, 72-, and 200-bar trusses

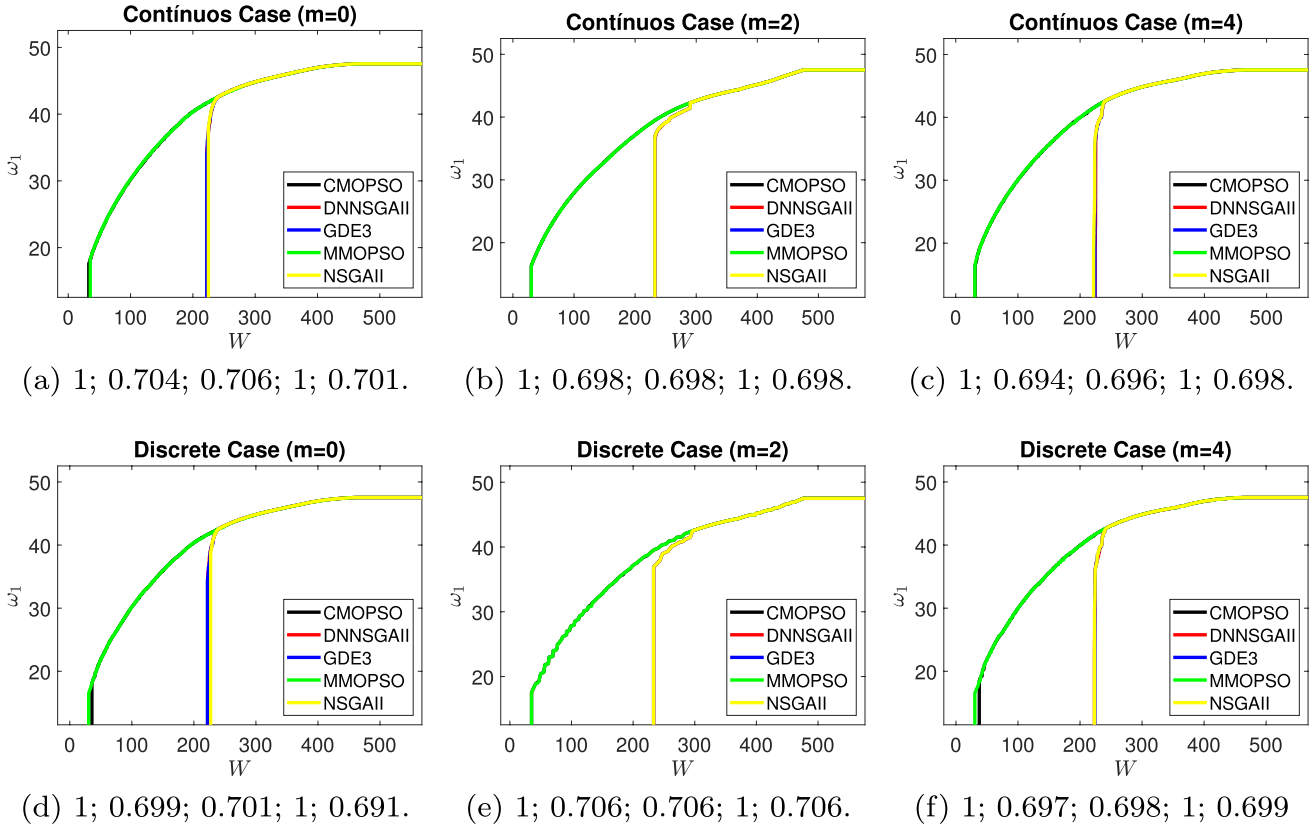

(a) 1; 0.704; 0.706; 1; 0.701. (b) 1; 0.698; 0.698; 1; 0.698. (c) 1; 0.694; 0.696; 1; 0.698.

(d) 1; 0.699; 0.701; 1; 0.691. (e) 1; 0.706; 0.706; 1; 0.706. (f) 1; 0.697; 0.698; 1; 0.699

Fig. 11 EAF_{best} solutions of the 25-bar truss. The values in each graph indicate the areas under the curve, normalized by the largest of them, in this order: CMOPSO; DN-NSGA-II; GDE3; MMOPSO; NSGA-II

(continuous and discrete cases), with indicators from the literature.

A set of non-dominated solutions was extracted from the experiments, and two analyses were conducted to evaluate these solutions. The first analysis evaluated the effect of using the cardinality constraints and the performance indicators. When the hypervolume and IGD+ metrics were analyzed, the CMOPSO algorithm achieved the best performance, followed by MMOPSO. For the Spacing metric, the best performance was obtained by NSGA-II, followed by the GDE3 and DN-NSGA-II algorithms, considering that the difference between them was very small. Finally, in terms of the overall performance, the CMOPSO algorithm obtained the best results, followed by the NSGA-II, DN-NSGA-II, GDE3, and MMOPSO algorithms, in that order.

The second analysis took into account the DM preferences about different criteria, conducted for the 72-bar truss (discrete case), and presented the objective function values of the MTD solutions, along with their respective design variables. Therefore, these results and the extracted solutions for all scenarios offer the DM several configurations for the 72-bar truss. Thus, it is up to him/her to choose the one that best meets his/her intentions.

Five algorithms were adopted to evaluate their performance in obtaining the multi-objective structural optimization problems discussed in this article. These approaches were used in PlatEMO, a platform widely used in the literature. Furthermore, these algorithms were selected based on those inspired by genetic algorithms, particle swarm optimization, and differential evolution. In this sense, three meta-heuristics were contemplated here, each with its particularity, being one of the most used and consolidated in evolutionary computation. A limitation of the current work is that the algorithms used can be contemplated by other variants.

The methodology used in this paper can be easily extended to problems with greater complexity both in the objective function and in the constraints in the context of real engineering optimization problems, such as those, concerning spatial frames. It is possible to expand the

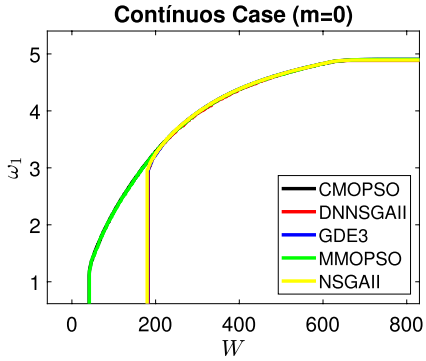

(a) 1; 0.911; 0.915; 0.999; 0.916.

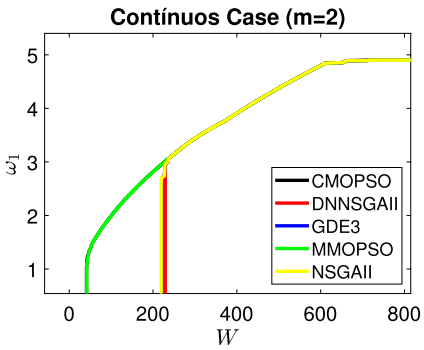

(b) 1; 0.869; 0.877; 0.999; 0.879.

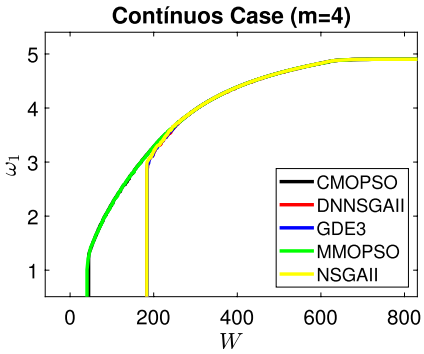

(c) 1; 0.905; 0.906; 1; 0.907.

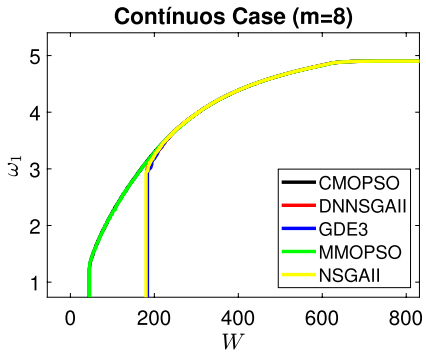

(d) 1; 0.918; 0.916; 0.999; 0.920.

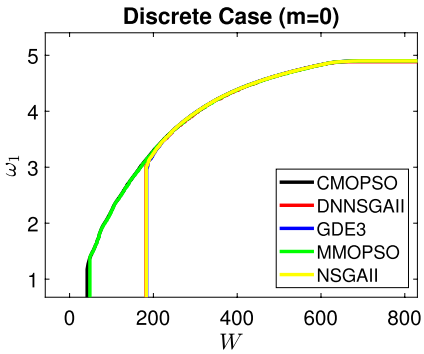

(e) 1; 0.914; 0.915; 0.998; 0.915.

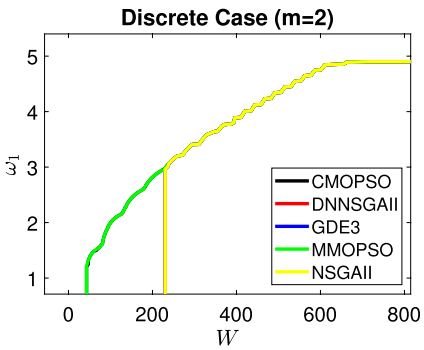

(f) 1; 0.882; 0.882; 1; 0.882.

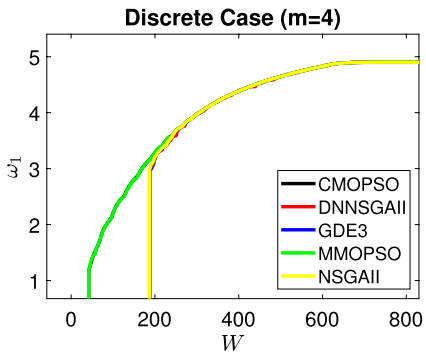

(g) 1; 0.908; 0.911; 1; 0.912.

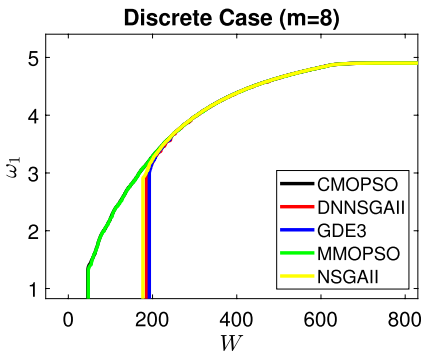

(h) 1; 0.917; 0.912; 0.999; 0.927.

Fig. 12 EAF_{best} solutions of the 72-bar truss. The values in each graph indicate the areas under the curve, normalized by the largest of them, in this order: CMOPSO; DN-NSGA-II; GDE3; MMOPSO; NSGA-II

formulations of structural optimization problems for more than two objectives by finding Pareto surfaces, such as the weight, the first natural frequency of vibration, and the maximum nodal displacement, as conflicting objective functions. Furthermore, it is also possible to investigate Pareto surface solution extraction techniques, such as those applied to identify preference regions of the DM used in this paper.

The present work's limitations are related to linear elastic materials, small displacements, and small deformations.

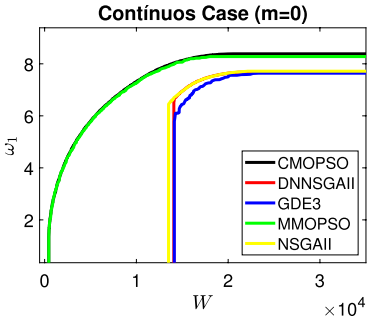

(a) 1; 0.471; 0.453; 0.991; 0.493.

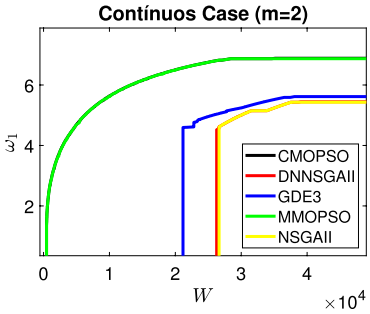

(b) 1; 0.264; 0.380; 0.999; 0.257.

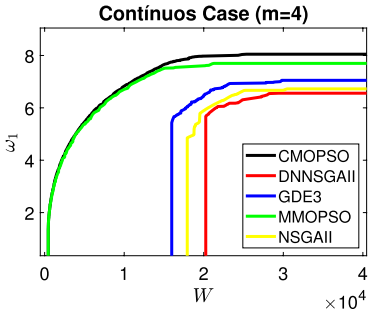

(c) 1; 0.298; 0.455; 0.962; 0.367.

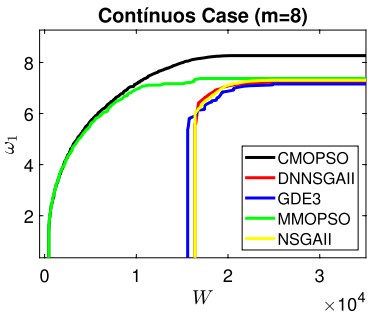

(d) 1; 0.349; 0.363; 0.911; 0.350.

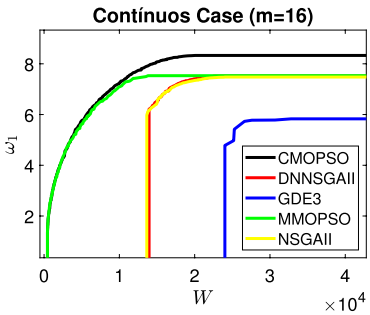

(e) 1; 0.579; 0.191; 0.917; 0.583.

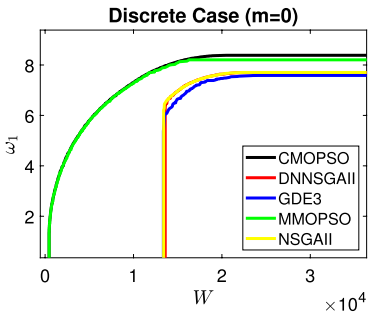

(f) 1; 0.516; 0.505; 0.986; 0.522.

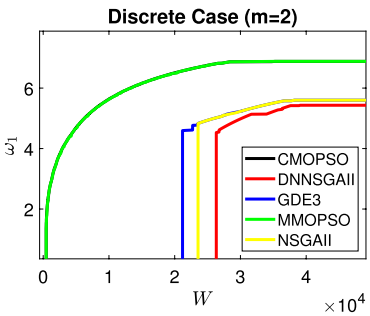

(g) 1; 0.263; 0.379; 0.999; 0.336.

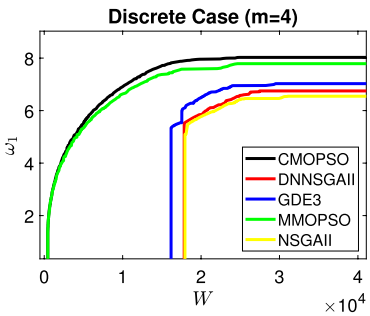

(h) 1; 0.381; 0.455; 0.953; 0.365.

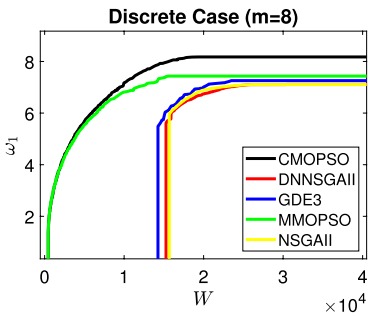

(i) 1; 0.474; 0.518; 0.914; 0.469.

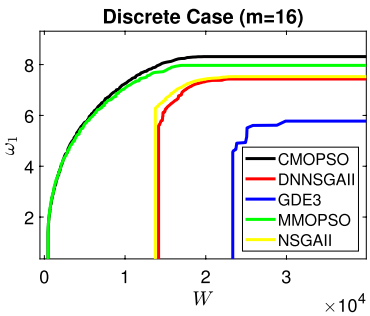

(j) 1; 0.526; 0.152; 0.961; 0.553.

Fig. 13 EAF_{best} solutions of the 200-bar truss. The values in each graph indicate the areas under the curve, normalized by the largest of them, in this order: CMOPSO; DN-NSGA-II; GDE3; MMOPSO; NSGA-II

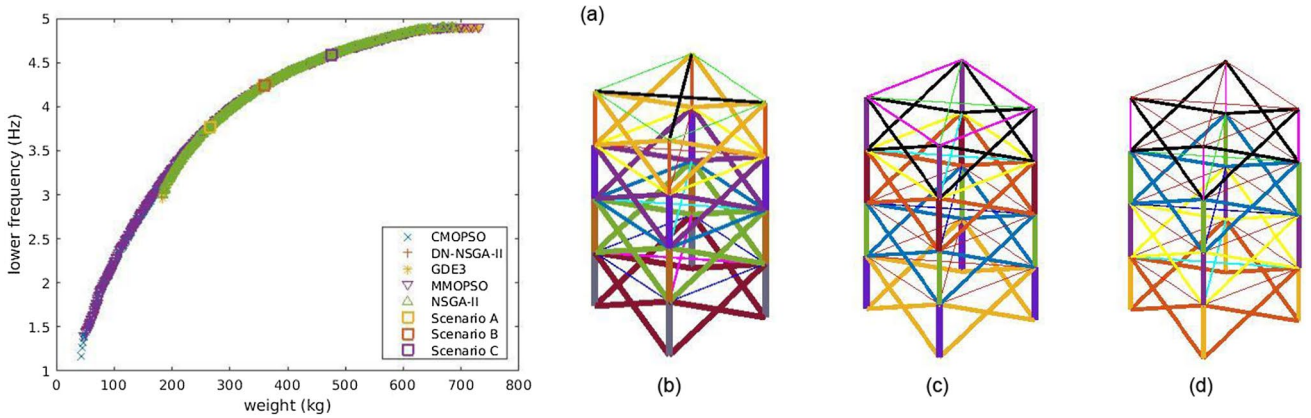

Fig. 14 **a** MTD solutions without set cardinality constraint to each scenario for the 72-bar truss (discrete case). Extracted solutions: **b** Scenario A, **c** Scenario B, and **d** Scenario C

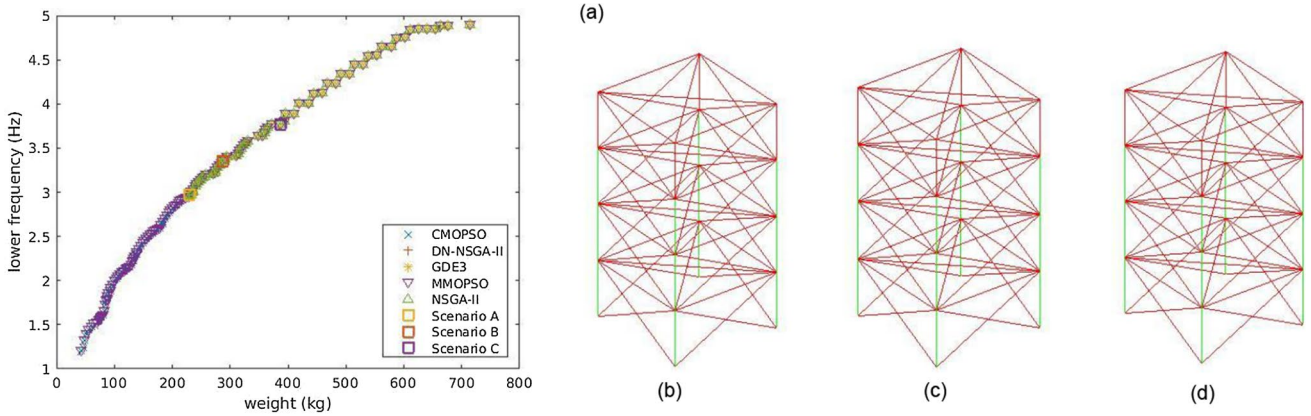

Fig. 15 **a** MTD solutions with $m = 2$ to each scenario for the 72-bar truss (discrete case). Extracted solutions: **b** Scenario A, **c** Scenario B, and **d** Scenario C

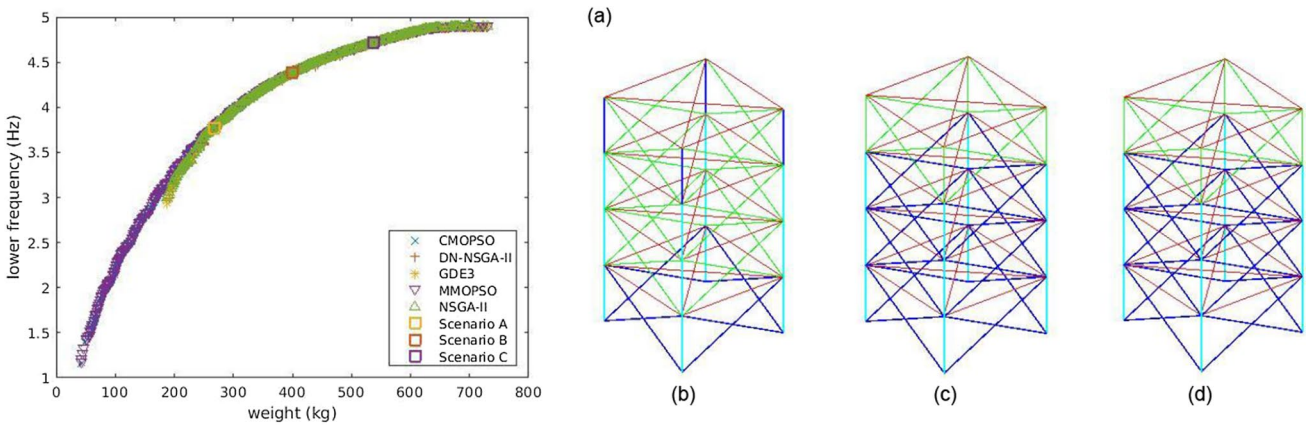

Fig. 16 **a** MTD solutions with $m = 4$ to each scenario for the 72-bar truss (discrete case). Extracted solutions: **b** Scenario A, **c** Scenario B, and **d** Scenario C

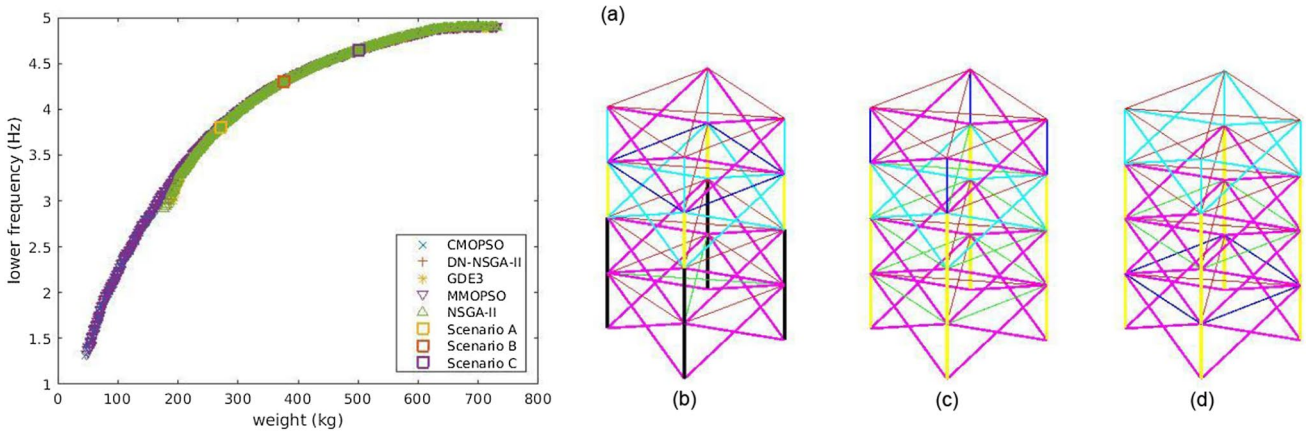

Fig. 17 **a** MTD solutions with $m = 8$ to each scenario for the 72-bar truss (discrete case). Extracted solutions: **b** Scenario A, **c** Scenario B, and **d** Scenario C

Table 7 Design variables (dv) and objective function values of the MTD solutions (Scenarios (Sc.) A, B, and C) of the 72-Bar truss (discrete case). $W(\mathbf{x})$ in kg and $\omega_1(\mathbf{x})$ in Hz

	No cardinality constraints			$m = 2$			$m = 4$			$m = 8$		
dv	Sc. A	Sc. B	Sc. C	Sc. A	Sc. B	Sc. C	Sc. A	Sc. B	Sc. C	Sc. A	Sc. B	Sc. C
A_1	6.0372	13.3738	16.8674	5.0936	6.4450	5.920	9.0593	13.6817	19.7562	8.2073	9.7823	17.8802
A_2	8.2478	11.8899	18.3729	5.0936	6.4450	5.9209	8.0063	13.6817	19.7562	9.1725	14.1213	17.8802
A_3	1.0035	1.1028	1.0000	5.0936	6.4450	5.9209	1.1277	1.0000	1.1024	1.0285	1.0000	1.0200
A_4	1.3677	1.0197	1.0000	5.0936	6.4450	5.9209	1.1277	1.0000	1.1024	1.0285	1.0000	1.0200
A_5	16.7794	24.9452	25.0000	16.2969	23.3654	23.4759	25.0000	25.0000	24.7684	20.3821	24.7632	25.0000
A_6	8.5076	12.9564	18.6816	5.0936	6.4450	5.9209	8.0063	14.8069	22.4605	8.2073	12.5844	20.0813
A_7	1.2924	1.1513	1.0000	5.0936	6.4450	5.9209	1.1277	1.000	1.1024	1.0605	1.0000	1.0200
A_8	1.0009	1.0906	1.1167	5.0936	6.4450	5.9209	1.1277	1.0000	1.1024	1.0285	1.2586	1.0200
A_9	24.9964	24.7065	24.9979	16.2969	23.3654	23.4759	25.0000	25.0000	24.7684	24.9047	24.7632	25.0000
A_{10}	8.5347	12.5107	18.3584	5.0936	6.4450	5.9209	8.0063	14.8069	22.4605	9.1725	14.1213	20.0813
A_{11}	1.3741	1.0000	1.0000	5.0936	6.4450	5.9209	1.1277	1.0000	1.1024	1.0285	1.2586	1.0964
A_{12}	1.1099	1.0301	1.2679	5.0936	6.4450	5.9209	1.1277	1.0000	1.1024	1.0285	1.0000	1.0200
A_{13}	24.7376	24.9765	24.6797	16.2969	23.3654	23.4759	25.0000	25.0000	24.7684	24.9047	24.7632	25.0000
A_{14}	9.3184	13.2965	19.3141	5.0936	6.4450	5.9209	9.0593	14.8069	24.7684	9.1725	14.1213	20.0813
A_{15}	1.0066	1.0000	1.0000	5.0936	6.4450	5.9209	1.1277	1.0000	1.1024	1.0285	1.2586	3.0673
A_{16}	1.2108	1.0000	1.2730	5.0936	6.4450	5.9209	1.1277	1.0000	1.1024	1.0566	1.0000	1.0200
$W(\mathbf{x})$	264.638	358.829	475.117	229.320	287.590	287.590	266.875	398.851	536.783	270.079	375.031	500.025
$\omega_1(\mathbf{x})$	3.7724	4.2417	4.5933	2.9743	3.3616	3.3616	3.7724	4.3844	4.7218	3.8075	4.3008	4.6482

There is no consideration of material and geometric nonlinearities or plastic deformations. The analyses have not yet been extended to structures with different loads, including dynamic actions and constraints established by standards.

Finally, future works are expected (i) to use a priori and interactive user preference information in the search engine for multi-objective optimization problems and (ii) to use metamodels to speed up the process of evaluating a candidate solution.

Funding The authors wish to thank CNPq (Conselho Nacional de Desenvolvimento Científico e Tecnológico), Grants No. 308105/2021-4 and 312682/2018-2, FAPEMIG (Fundação de Amparo à Pesquisa do Estado de Minas Gerais), Grants No. TEC APQ 00103-12, TEC APQ 00337-18, TEC PPM 00174-18, and TEC APQ 00408-21, and CAPES (Coordenação de Aperfeiçoamento de Pessoal de Nível Superior) for their support.

Data Availability Not applicable

Code Availability Codes can be requested from the corresponding author upon request.

Declarations

Conflict of interest The authors declare that they have no known competing financial interests or personal relationships that could have appeared to influence the work reported in this paper.

References

1. Angelo JS, Bernardino HS, Barbosa HJ (2015) Ant colony approaches for multiobjective structural optimization problems with a cardinality constraint. Adv Eng Softw 80:101–115
2. Assimi H, Jamali A, Nariman-Zadeh N (2019) Multi-objective sizing and topology optimization of truss structures using genetic programming based on a new adaptive mutant operator. Neural Comput Appl 31(10):5729–5749
3. Barbosa HJ, Lemonge AC, Borges CC (2008) A genetic algorithm encoding for cardinality constraints and automatic variable linking in structural optimization. Eng Struct 30(12):3708–3723
4. Barbosa HJC, Bernardino HS, Barreto AMS (2010) Using performance profiles to analyze the results of the 2006 cec constrained optimization competition. In: 2010 IEEE world congress on computational intelligence - WCCI, pp. 1–8
5. Barbosa HJC, Lemonge ACC (2005) A genetic algorithm encoding for a class of cardinality constraints. In: Proceedings of the 7th annual conference on genetic and evolutionary computation, pp. 1193–1200. ACM Press
6. Barbosa HJC, Lemonge ACC, Borges CCH (2008) A genetic algorithm encoding for cardinality constraints and automatic variable linking in structural optimization. Eng Struct 30:3708–3723
7. Bathe KJ (2006) Finite element procedures. Prentice Hall, Pearson Education Inc
8. Brans JP, Vincke P, Mareschal B (1986) How to select and how to rank projects: the promethee method. Eur J Oper Res 24(2):228–238
9. Carvalho JPG, Carvalho ÉCR, Vargas DEC, Hallak PH, Lima BSLP, Lemonge ACC (2021) Multi-objective optimum design of truss structures using differential evolution algorithms. Comput Struct 252:106544
10. Carvalho JPG, Lemonge ACC, Carvalho ÉCR, Hallak PH, Bernardino HS (2018) Truss optimization with multiple frequency constraints and automatic member grouping. Struct Multidiscip Optim 57(2):547–577
11. Chou JS, Truong DN (2022) Multiobjective forensic-based investigation algorithm for solving structural design problems. Autom Constr 134:104084
12. Coello CAC, Lamont GB, Veldhuizen DAV (2007) Evolutionary algorithms for solving multi-objective problems (genetic and evolutionary computation), 2nd edn. Springer-Verlag, New York Inc
13. Coello Coello CA, Reyes Sierra M (2004) A study of the parallelization of a coevolutionary multi-objective evolutionary algorithm. In: Mexican international conference on artificial intelligence, pp. 688–697. Springer
14. Colorni A, Dorigo M, Maniezzo V et al (1991) Distributed optimization by ant colonies. In: Proceedings of the first european conference on artificial life, vol. 142, pp. 134–142. Paris, France
15. Deb K, Pratap A, Agarwal S, Meyarivan T (2002) A fast and elitist multiobjective genetic algorithm: NSGA-II. IEEE Trans Evol Comput 6(2):182–197
16. Deveci K, Güler Ö (2020) A CMOPSO based multi-objective optimization of renewable energy planning: case of turkey. Renew Energy 155:578–590
17. Dolan ED, More J (2002) Benchmarking optimization software with performance profiles. Math Program 91:201–213
18. Eberhart R, Kennedy J (1995) A new optimizer using particle swarm theory. In: Micro Machine and Human Science, 1995. MHS'95, Proceedings of the sixth international symposium on, pp. 39–43. IEEE
19. Edwards W, Barron FH (1994) Smarts and smarter: improved simple methods for multiattribute utility measurement. Organ Behav Hum Decis Process 60(3):306–325
20. Eid H, Garcia-Hernandez L, Abraham A (2022) Spiral water cycle algorithm for solving multi-objective optimization and truss optimization problems. Eng Comput 38:963–973
21. Fonseca CM, Fleming PJ (1996) On the performance assessment and comparison of stochastic multiobjective optimizers. In: International conference on parallel problem solving from nature, pp. 584–593. Springer
22. Gellatly RA, Berke L (1971) Optimal structural design. Tech. rep, DTIC Document
23. Ghasemi M, Hinton E, Wood R (1999) Optimization of trusses using genetic algorithms for discrete and continuous variables. Eng Comput 16(3):272–303
24. Gholizadeh S, Asadi H, Baghchevan A (2014) Optimal design of truss structures by improved multi-objective firefly and bat algorithms. Iran Univ Sci Technol 4(3):415–431
25. Greiner D, Galván B, Emperador JM, Méndez M, Winter G (2011) Introducing reference point using g-dominance in optimum design considering uncertainties: an application in structural engineering. In: International conference on evolutionary multi-criterion optimization, pp. 389–403. Springer
26. Greiner D, Hajela P (2012) Truss topology optimization for mass and reliability considerations - Co-evolutionary multiobjective formulations. Struct Multidiscip Optim 45(4):589–613
27. Greiner D, Winter G, Emperador JM, Galván B (2005) Gray coding in evolutionary multicriteria optimization: Application in frame structural optimum design. In: International conference on evolutionary multi-criterion optimization, pp. 576–591. Springer
28. Hayyolalam V, Kazem AAP (2020) Black widow optimization algorithm: a novel meta-heuristic approach for solving engineering optimization problems. Eng Appl Artif Intell 87:103249
29. He Z, Xiong X, Yang B, Li H (2022) Aerodynamic optimisation of a high-speed train head shape using an advanced hybrid surrogate-based nonlinear model representation method. Optim Eng 23:59–84
30. Herencia JE, Haftka RT (2010) Structural optimization with limited number of element properties. Struct Multidiscip Optim 41(5):817–820
31. Herencia JE, Haftka RT, Balabanov V (2013) Structural optimization of composite structures with limited number of element properties. Struct Multidiscip Optim 47(2):233–245
32. Holland JH (1973) Genetic algorithms and the optimal allocation of trials. SIAM J Comput 2(2):88–105
33. Hosseini SS, Hamidi SA, Mansuri M, Ghoddosian A (2015) Multi objective particle swarm optimization (MOPSO) for size and shape optimization of 2D truss structures. Periodica Polytechnica Civil Eng 59(1):9
34. Hughes TJ (2012) The finite element method: linear static and dynamic finite element analysis. DoverPublications.com

35. Ishibuchi H, Masuda H, Tanigaki Y, Nojima Y (2015) Modified distance calculation in generational distance and inverted generational distance. In: International conference on evolutionary multi-criterion optimization, pp. 110–125. Springer
36. Jha SB, Jha JK, Tiwari MK (2019) A multi-objective meta-heuristic approach for transit network design and frequency setting problem in a bus transit system. Comput Ind Eng 130:166–186
37. Kaveh A, Ghazaan MI (2016) Optimal design of dome truss structures with dynamic frequency constraints. Struct Multidiscip Optim 53(3):605–621
38. Kaveh A, Ghazaan MI (2019) A new VPS-based algorithm for multi-objective optimization problems. Eng Comput 36:1029–1040
39. Kaveh A, Laknejadi K (2013) A hybrid evolutionary graph-based multi-objective algorithm for layout optimization of truss structures. Acta Mech 224(2):343–364
40. Kaveh A, Mahdavi VR (2019) Multi-objective colliding bodies optimization algorithm for design of trusses. J Comput Des Eng 6(1):49–59
41. Kaveh A, Massoudi M (2014) Multi-objective optimization of structures using charged system search. Sci Iran Trans A Civil Eng 6:1845–60
42. Khalkhali A, Khakshournia S, Nariman-Zadeh N (2014) A hybrid method of fem, modified NSGAII and TOPSIS for structural optimization of sandwich panels with corrugated core. J Sandwich Struct Mater 16(4):1099636214531516
43. Khodadadi N, Talatahari S, Dadras Eslamlou A (2022) MOTEO: a novel multi-objective thermal exchange optimization algorithm for engineering problems. Soft Comput 26:6659–6684
44. Kripka M, Medeiros GF, Lemonge ACC (2013) Structural optimization of reinforced concrete building grillages considering cardinality constraints. In: 10th World congress on structural and multidisciplinary optimization, pp. 01–06
45. Kripka M, Medeiros GF, Lemonge ACC (2015) Use of optimization for automatic grouping of beam cross-section dimensions in reinforced concrete building structures. Eng Struct 99:311–8
46. Kukkonen S, Lampinen J (2005) Gde3: The third evolution step of generalized differential evolution. In: 2005 IEEE Congress on evolutionary computation, vol. 1, pp. 443–450. IEEE
47. Kumar S, Tejani GG, Pholdee N, Bureerat S (2020) Multi-objective modified heat transfer search for truss optimization. Eng Comput 37:3439–3454
48. Lemonge AC, Barbosa HJ (2004) An adaptive penalty scheme for genetic algorithms in structural optimization. Int J Numer Meth Eng 59(5):703–736
49. Lemonge AC, Carvalho JP, Hallak PH, Vargas DE (2021) Multi-objective truss structural optimization considering natural frequencies of vibration and global stability. Expert Syst Appl 165:113777
50. Lemonge ACC, Barbosa HJC, Coutinho ALGA, Borges CCH (2011) Multiple cardinality constraints and automatic member grouping in the optimal design of steel framed structures. Eng Struct 33(2):433–444
51. Lemonge ACC, Barbosa HJC, da Fonseca LG, Coutinho ALGA (2010) A genetic algorithm for topology optimization of dome structures. In: Proceedings of the 2nd international conference on engineering optimization EngOpt
52. Li M, Yao X (2019) Quality evaluation of solution sets in multiobjective optimisation: A survey. ACM Comput Surv (CSUR) 52(2):1–38
53. Liang JJ, Yue C, Qu BY (2016) Multimodal multi-objective optimization: A preliminary study. In: 2016 IEEE Congress on evolutionary computation (CEC), pp. 2454–2461. IEEE
54. Lin Q, Li J, Du Z, Chen J, Ming Z (2015) A novel multi-objective particle swarm optimization with multiple search strategies. Eur J Oper Res 247(3):732–744
55. Liu X, Cheng G, Wang B, Lin S (2012) Optimum design of pile foundation by automatic grouping genetic algorithms. ISRN Civil Eng 2012:1–17
56. Liu X, Cheng G, Yan J, Jiang L (2012) Singular optimum topology of skeletal structures with frequency constraints by AGGA. Struct Multidiscip Optim 45(3):451–466
57. Liu Y, Ishibuchi H, Nojima Y, Masuyama N, Shang K (2018) A double-niched evolutionary algorithm and its behavior on polygon-based problems. In: International conference on parallel problem solving from nature, pp. 262–273. Springer
58. López-Ibánez M, Paquete L, Stützle T (2010) Exploratory analysis of stochastic local search algorithms in biobjective optimization. In: Bartz-Beielstein T, Chiarandini M, Paquete L, Preuss M (eds) Experimental methods for the analysis of optimization algorithms. Springer, Berlin, Germany, pp 209–222
59. Lorusso A, Guida D (2022) IoT system for structural monitoring. In: Karabegović I, Kovačević A, Mandžuka S (eds) New technologies, development and application v. Springer International Publishing, Cham, pp 599–606
60. Maity K, Sengupta R, Saha S (2019) MM-NAEMO: Multimodal neighborhood-sensitive archived evolutionary many-objective optimization algorithm. In: 2019 IEEE Congress on evolutionary computation (CEC), pp. 286–294. IEEE
61. McGuire W, Gallagher RH, Ziemian RD (2014) Matrix structural analysis. John Wiley & Sons, New York . 2nd Edition
62. Mei L, Wang Q (2021) Structural optimization in civil engineering: a literature review. Buildings 11(2):66
63. Mokarram V, Banan MR (2018) An improved multi-objective optimization approach for performance-based design of structures using nonlinear time-history analyses. Appl Soft Comput 73:647–665
64. Mokarram V, Banan MR (2018) A new PSO-based algorithm for multi-objective optimization with continuous and discrete design variables. Struct Multidiscip Optim 57(2):509–533
65. Noilublao C, Bureerat S (2009) Simultaneous topology, shape and sizing optimisation of skeletal structures using multiobjective evolutionary algorithms. In: Evolutionary computation. IntechOpen
66. Noilublao N, Bureerat S (2011) Simultaneous topology, shape and sizing optimisation of a three-dimensional slender truss tower using multiobjective evolutionary algorithms. Comput Struct 89(23–24):2531–2538
67. Özkan R, Genç MS (2021) Multi-objective structural optimization of a wind turbine blade using NSGA-II algorithm and FSI. Aircr Eng Aerosp Technol 93(6):1029–1042
68. Pal M, Bandyopadhyay S (2019) Differential evolution for multimodal multi-objective problems. In: Proceedings of the genetic and evolutionary computation conference companion, pp. 1399–1406
69. Parreiras R, Vasconcelos J (2009) Decision making in multiobjective optimization aided by the multicriteria tournament decision method. Nonlinear Anal Theory Methods Appl 71(12):e191–e198
70. Patil MV, Kulkarni AJ (2020) Pareto dominance based multiobjective cohort intelligence algorithm. Inf Sci 538:69–118
71. Połap D, Woźniak M (2021) Red fox optimization algorithm. Expert Syst Appl 166:114107
72. Rajeev S, Krishnamoorthy C (1992) Discrete optimization of structures using genetic algorithms. J Struct Eng 118(5):1233–1250
73. Richardson JN, Adriaenssens S, Bouillard P, Coelho RF (2012) Multiobjective topology optimization of truss structures with kinematic stability repair. Struct Multidiscip Optim 46(4):513–532

74. Saaty TL (1980) The analytic hierarchy process, vol. 324. McGraw-Hill
75. Sarah J, Hejazi F, Rashid RS, Ostovar N (2019) A review of dynamic analysis in frequency domain for structural health monitoring. IOP Conf Ser Earth Environ Sci 357(1):012007
76. Schott JR (1995) Fault tolerant design using single and multicriteria genetic algorithm optimization. Master's thesis, Department of aeronautics and astronautics, massachusetts institute of technology
77. Spytek J, Machynia A, Dziedziech K, Dworakowski Z, Holak K (2023) Novelty detection approach for the monitoring of structural vibrations using vision-based mean frequency maps. Mech Syst Signal Process 185:109823
78. Storn R, Price K (1995) Differential evolution a simple and efficient adaptive scheme for global optimization over continuous spaces. Tech Rep Univ 4:341–59
79. Storn R, Price K (1997) Differential evolution-a simple and efficient heuristic for global optimization over continuous spaces. J Global Optim 11(4):341–359
80. Storn R, Price K (1997) Differential evolution a simple and efficient adaptive scheme for global optimization over continuous spaces. J Global Optim 11(4):341–359
81. Su R, Wang X, Gui L, Fan Z (2011) Multi-objective topology and sizing optimization of truss structures based on adaptive multi-island search strategy. Struct Multidiscip Optim 43(2):275–286
82. Tejani GG, Kumar S, Gandomi AH (2021) Multi-objective heat transfer search algorithm for truss optimization. Eng Comput 37:641–662
83. Tejani GG, Pholdee N, Bureerat S, Prayogo D (2018) Multiobjective adaptive symbiotic organisms search for truss optimization problems. Knowl-Based Syst 161:398–414
84. Tejani GG, Pholdee N, Bureerat S, Prayogo D, Gandomi AH (2019) Structural optimization using multi-objective modified adaptive symbiotic organisms search. Expert Syst Appl 125:425–441
85. Tian Y, Cheng R, Zhang X, Jin Y (2017) PlatEMO: A MATLAB platform for evolutionary multi-objective optimization. IEEE Comput Intell Mag 12(4):73–87
86. Vargas DE, Lemonge AC, Barbosa HJ, Bernardino HS (2019) Differential evolution with the adaptive penalty method for structural multi-objective optimization. Optim Eng 20(1):65–88
87. Vargas DE, Lemonge AC, Barbosa HJ, Bernardino HS (2021) Solving multi-objective structural optimization problems using GDE3 and NSGA-II with reference points. Eng Struct 239:112187
88. Venkayya V (1971) Design of optimum structures. Comput Struct 1(1):265–309
89. Vo-Duy T, Duong-Gia D, Ho-Huu V, Nguyen-Thoi T (2020) An effective couple method for reliability-based multi-objective optimization of truss structures with static and dynamic constraints. Int J Comput Methods 17(06):1950016
90. Xie L, Tang H, Hu C, Xue S (2016) An adaptive multi-objective immune algorithm for optimal design of truss structures. J Asian Archit Build Eng 15(3):557–564
91. Yang Q, Wang Z, Luo J, He Q (2021) Balancing performance between the decision space and the objective space in multimodal multiobjective optimization. Memet Comput 13(1):31–47
92. Yang Y, Zhu Z, Au SK (2023) Bayesian dynamic programming approach for tracking time-varying model properties in shm. Mech Syst Signal Process 185:109735
93. Zhang Q, Chen JC, Chong PP (2004) Decision consolidation: criteria weight determination using multiple preference formats. Decis Support Syst 38(2):247–258
94. Zhang X, Liu H, Tu L, Zhao J (2020) An efficient multi-objective optimization algorithm based on level swarm optimizer. Math Comput Simul 177:588–602
95. Zhang X, Zheng X, Cheng R, Qiu J, Jin Y (2018) A competitive mechanism based multi-objective particle swarm optimizer with fast convergence. Inf Sci 427:63–76
96. Zhou A, Qu BY, Li H, Zhao SZ, Suganthan PN, Zhang Q (2011) Multiobjective evolutionary algorithms: A survey of the state of the art. Swarm Evol Comput 1(1):32–49
97. Zitzler E, Thiele L (1999) Multiobjective evolutionary algorithms: a comparative case study and the strength pareto approach. IEEE Trans Evol Comput 3(4):257–271